

REVIEWS OF TOPICAL PROBLEMS

PACS numbers: 81.05.ug, 81.15.Aa, 81.15.Gh

Problems in homoepitaxial growth of diamonds using CVD method and ways to solve them

R.A. Khmelnitsky, N.B. Rodionov, A.G. Trapeznikov, V.P. Yartsev, V.P. Rodionova, A.N. Kirichenko, A.V. Krasilnikov

DOI: https://doi.org/10.3367/UFNe.2024.06.039692

Contents

Abstract. **The CVD technology of homoepitaxial growth of single-crystal diamond has experienced significant difficulties for more than a decade. Long-term morphologically stable epitaxy of the crystal is not possible: as the crystal grows, a surface relief develops; over time, polycrystals inevitably appear on the growth surface, a polycrystalline 'rim' grows on the edges, and structural perfection of the material is not achieved. Productive epitaxy on the {111} faces is impossible due to unavoidable twinning. Considered an achievement is the growth of 1–2 mm of epitaxial material in a single session on a well-prepared facet vicinal to (001). To obtain significant growth of a crystal, it is necessary to periodically extract it from the reactor, trim the polycrystalline rim along the perimeter, and re-polish the growth surface for a new growth session. The brilliant prospects of using CVD diamond are still very poorly realized. These problems urgently require a solution. It is now clear that the structural perfection of the material is inextricably linked with the achievement of morphologically stable epitaxial growth. To analyze the mechanism of growth of single-crystal diamond using the CVD method, a model of layered growth was used. It provided a description of such key components of the growth surface as sources of layered growth and a stairway of growth ledges. The morphological instability of layered growth is mainly due to (a) positive feedback related to the action of a boundary diffusion layer with a large concentration gradient of growth radicals and (b) the Ehrlich–Schwoebel barrier for the movement of adatoms over the growth step edge. Morphological instability of homoepitaxial diamond growth primarily manifests itself in the grouping of steps (with the formation of macrosteps), meandering of steps, emergence of hillocks and mounds, and formation of depressions. These destructive phenomena have been shown to arise and develop during epitaxy on the faces close to {100}. The development of the growth surface relief inevitably leads to the appearance of twins on it, i.e., to the breakdown of epitaxy. Diagnosing mechanisms of morphological instability of diamond epitaxy by means of the CVD method made it possible to suggest ways to eliminate it. They include: (a) the creation of controlled sources of layered growth; (b) the preparation of a growth ledge stairway by correct polishing of growth faces; (c) the choice of the optimal vicinal angle of growth surfaces; and (d) the selection of supersaturation conditions for morphologically stable operation of layered growth sources and the development of growth layers.**

Keywords: synthetic diamond, epitaxy, CVD

R.A. Khmelnitsky [1, 2, *], **N.B. Rodionov** [2], **A.G. Trapeznikov** [2], **V.P. Yartsev** [2], **V.P. Rodionova** [2], **A.N. Kirichenko** [2], **A.V. Krasilnikov** [2]
[1] Lebedev Physical Institute, Russian Academy of Sciences, Leninskii prosp. 53, 119991 Moscow, Russian Federation
[2] ITER Project Center, enterprise of the Rosatom State Corporation, pl. Akademika Kurchatova 1, str. 3, 123182 Moscow, Russian Federation
E-mail: [*] khmelnitskyra@lebedev.ru

Received 8 December 2023, revised 20 May 2024
Uspekhi Fizicheskikh Nauk **195** (1) 3 – 33 (2025)
Translated by M Zh Shmatikov

1. Homoepitaxy of diamond using CVD method

The first successful attempts to grow diamond from the gas phase were made in the 1950s. It is reported in [1] that B.V. Spitsyn and B.V. Deryagin filed a patent application for the formation of diamond by pyrolysis of CBr_4 and CI_4 in 1956, although the patent was issued only in 1980 [2]. In 1958, an application for a patent was filed in the USA on the cyclic process of pyrolysis of gaseous hydrocarbons and diamond growth at low pressures [3]. This activity was continued and developed in [4]. In 1981 and 1982, a qualitative leap was made in Chemical Vapor Deposition (CVD) technology of diamond growth from the gas phase [5, 6]. A mixture of hydrogen and hydrocarbon was used, which was activated by a highly heated tungsten filament. Production of diamond films grown on nondiamond substrates located close to the hot filament began. Due to the presence of atomic hydrogen in the gas phase, graphite formed simultaneously with diamond was etched. This technology made it possible to abandon the alternation of growth and etching cycles, and greatly increased the diamond growth rate, enabling its industrial applications [7]. Since then, many methods for activating the gas mixture have been developed, up to the creation of plasma and the use of powerful burners and plasma torches, but the CVD principle remains the same. The main option for homoepitaxial diamond growth is microwave (MW) CVD technology, which allows the purest and most perfect material to be grown.

We review the current state of diamond homoepitaxy technology based on the CVD method, presenting the difficulties it has encountered. Growth experiments were carried out to identify the main patterns and approaches to overcome problems. The analysis of the results is based on the theory of layered crystal growth. This made it possible to find ways to overcome the difficulties of diamond homoepitaxy.

The CVD diamond process includes the following main phenomena [8]: introduction of gases into the reactor, the thermal or plasma activation of reagents [9], transfer of active radicals and molecules to the growing surface and their return to the gas environment, chemical and diffusion processes on the surface, and formation of sp^3 and sp^2 forms of carbon. A hydrocarbon (usually methane), heavily diluted with hydrogen, is used as a carbon source. The pressure of the gas mixture in the reactor is maintained in the range of tens of and several hundred Torr. By means of thermal and chemical activation, the gas mixture can be heated to 3500 K or higher; with electromagnetic RF (radio frequency) or microwave excitation, the gas is ionized and a plasma jet or cloud is formed. In the latter case, the temperature of the electron gas can exceed 10,000 K, and its density is $(1-10)\times 10^{11}$ cm^{-3} [10]. Electrons absorb most of the microwave energy and transfer it to molecules in collisions, which leads to the formation of hydrogen radicals and hydrocarbons — key agents in diamond growth. In general, the concentration of charged atoms, molecules, and radicals in such plasma is small and insignificant for the growth mechanisms. This is also evidenced by the success of the method of gas excitation by means of a heated filament, when the density of charged particles is negligible. The substrate temperature during diamond growth is 700–1300 °C.

The main agent in the CVD process is the hydrogen radical, atomic hydrogen H. Even in a purely hydrogen heated gas (especially with microwave excitation), many processes occur. In [11], 22 reactions are described, and in [12], 27 reactions involving molecular and atomic hydrogen are mentioned. Naturally, dissociation reactions are counteracted by recombination reactions. The role of hydrogen in CVD diamond growth is diverse and significant [11].

Atomic hydrogen is formed in plasma mainly due to the following chemical dissociation reactions:

$$e + H_2 \rightarrow H + H + e\,, \tag{1}$$

$$H_2 + H_2 \leftrightarrow H_2 + H + H\,, \tag{2}$$

$$H_2 + H \rightarrow H + H + H\,. \tag{3}$$

If a hydrocarbon is added to the plasma, the number of different reactions already exceeds a hundred [11]. Moreover, the type of initial hydrocarbon is not of great importance, since, in a typical microwave CVD plasma, a certain ratio of neutral particles, radicals, and ions is established, which is determined partly by collisions with electrons, but primarily by the temperature of the gas component. At present, in CVD technology, the methyl radical CH_3 is recognized as the main gas-phase source of diamond growth, although the heated gas contains other hydrocarbon radicals in higher concentrations (see Fig. 3b below). The methyl radical is formed in the plasma partly by electron impact, but mainly as a result of a chemical reaction involving atomic hydrogen:

$$CH_4 + H \leftrightarrow CH_3 + H_2\,. \tag{4}$$

In the most general form, the main chemical reactions involving atomic hydrogen and the methyl radical on the diamond growth surface are [13, 14]

$$C_DH + H \rightarrow C_D^* + H_2\,, \tag{5}$$

$$C_D^* + H \rightarrow C_DH\,, \tag{6}$$

$$C_D^* + CH_3 \rightarrow C_D\text{-}CH_3 \rightarrow C_DH + H_2\,, \tag{7}$$

$$C_D - CH_3 + H \rightarrow C_D^* + CH_4\,. \tag{8}$$

Here, C_D is a carbon atom on the diamond surface, C_D^* is a carbon atom on the diamond surface with a free bond, C_DH is a carbon atom on the diamond surface with a bond saturated with a hydrogen atom, and $C_D - CH_3$ is a carbon atom with a bond saturated with a methyl radical CH_3. Reaction (5) describes the formation of an open position with a free bond of a carbon atom on the diamond surface; reaction (6) is the saturation of this bond with atomic hydrogen; reaction (7) is the saturation of this bond with a hydrocarbon radical with the formation of an adatom, ultimately leading to the growth of the diamond phase; and reaction (8) is the etching of the adatom, returning carbon to the gas phase in the form of a hydrocarbon. The temperature dependences of the constants of these reactions are known [15]. In the approximation of a small fraction of hydrocarbons in the growth medium, the fraction of carbon atoms on the diamond surface with a free bond (C_D^*) is determined by the ratio of the constants of reactions (5) and (6) and depends only on the substrate temperature. In Section 4.1, the main processes occurring on the growth surface are described in more detail. It should be noted that the driving force of crystallization (depending primarily on supersaturation) is determined by the ratio of the rates of adsorption of hydrocarbon radicals (methyl radical — reaction (7)) on the growth surface from the gas phase and their desorption back into the gas phase, which is, actually, not evaporation, but etching (reaction (8)). In this case, the adsorption rate depends on the concentration of

hydrocarbon radicals (methyl radical) in the gas phase, and the etching rate depends on the concentration of the hydrogen radical (i.e., atomic hydrogen) [16]. In homoepitaxy, the driving force of crystallization is small (see Section 2 and Fig. 5), and the rate of hydrocarbon adsorption only slightly exceeds the rate of their desorption.

Polycrystalline films grown by the CVD method have already been applied in technology [17–19]. However, the main modern prospects for diamond [20–22] are associated with the need to grow high-quality and large-sized single-crystal material, and CVD technology in this regard has a promising advantage over the High Pressure High Temperature (HPHT) method [23, 24]. The introduction of diamond into modern electronics, and especially optics, requires the use of microelectronic technologies focused on photolithography methods. The main problems in this area are the unavailability of single-crystal diamond in the form of plates suitable for photolithography technology, its high cost, and low crystalline perfection of the material.

The general trend in microwave CVD technology is to increase the gas pressure and discharge power, which also makes it possible to increase the proportion of methane in the mixture and, ultimately, the deposition rate of diamond material [25, 26]. Further, we almost exclusively consider diamond growth by the CVD method with microwave plasma activation. This technique is now dominant in high-quality single-crystal diamond growth [27] due to the high growth rate and good purity of the grown material. However, all the phenomena and regularities described below are observed when other types of CVD technology (growth with a hot filament, DC plasma, various torches and plasma generators) are used [28–30], once again confirming the similarity of phenomena during diamond growth from the gas phase.

To illustrate the growth phenomena for this review, several experimental substrates of various shapes were made and CVD diamond was grown on them in a Plassys microwave reactor with the following growth parameters: gas pressure: 260 mbar, discharge power: 3 kW, methane content in the gas mixture: 2–5% (the rest is hydrogen), substrate temperature: $1030 \pm 20\,^{\circ}\mathrm{C}$. Some experiments were done with nitrogen added. Further, all figures where no references to sources are indicated present our results.

1.1 Morphology of single-crystal diamonds grown by CVD on (001) plates

Conventionally, wafers with a polished upper side close to the (001) face and unpolished lateral {110} facets are used for diamond homoepitaxy using CVD. They are cut from cuboctahedral crystals, usually relatively inexpensive, synthetic, and grown by the HPHT method. This method uses the maximum of the substrate material and provides maximum areas of epitaxial growth. At present, substrates are cut from HPHT crystals almost exclusively by laser cutting. The lateral sides are usually cut vertically. This allows the removal of {111} growth facets (which, as shown below, are extremely undesirable for epitaxy) and cutting off defective areas with inclusions and cracks. As a result of such cutting, the lateral, rough sides belong to the {110} system. The (001) faces of the wafer are polished.

The experience of dozens of scientific teams and production companies has shown that the use of standard (001) substrates yields poor epitaxy control and fails to provide morphologically stable growth and the structural perfection of the epitaxial material. As growth proceeds, the relief of the growth surface develops due to the grouping of steps, the superposition of growth layers from different directions from various local growth sources, and the formation and expansion of relief elements. Over time, the side facets of the substrate along its entire perimeter are covered with twins, which, as their number and size increase, grow together into a continuous layer of polycrystalline diamond, called a 'rim,' and twins inevitably appear on the growth surface — this implies the failure of epitaxy [31–33]. Sometimes, the crystal even cracks under the influence of the polycrystalline rim [34].

The formation of a polycrystalline rim along the perimeter of the plate is a significant factor limiting the growth of thick epitaxial diamond layers. In fact, the rim is formed by twin crystallites. The reason is that unpolished facets inevitably contain areas with facets close to {111}, which are prone to twinning. Twins are known to create mechanical stresses [35, 36]. Multiple twinning leads to the propagation of increasing mechanical stresses into the growing homoepitaxial film and substrate. The growth of a polycrystalline rim adversely affects the growth of the epitaxial material and often even leads to cracking of the entire crystal.

To prevent or at least slow down the formation of a polycrystalline rim and balance the growth conditions along the main, upper growth face of the wafer, it is proposed to place the substrate in a recess in the substrate holder to prevent the penetration of growth radicals into the gap and at the same time to balance the electromagnetic field in the horizontal plane to level the plasma parameters [37–41].

Much effort is being put into finding the optimal size of the recess and the gap between its walls and the substrate [42]. In [43], a recess in the form of an inverse truncated pyramid was used. This solution helps for a while [44], but, since the substrate grows upward and in width, for example, in [45], it was necessary to change the substrate holders three times with increasing recess sizes. This technique allows one to solve the problem of polycrystalline rim formation for awhile and increase the lateral dimensions of the crystal.

The second option is to cover the side facets with a neutral, stable, adhesive-strong coating on which neither diamond nor graphite grows. The difficult task of selecting such a coating [17, 46] is also encountered in attempts to use lithography for epitaxy, including a sophisticated method of reducing the density of growth dislocations in an epitaxial material due to epitaxial lateral overgrowth (ELO) [47]. Even such an expensive recipe can only delay the formation of a polycrystalline rim for awhile, because the upward growth of the substrate opens up unprotected areas along the perimeter for the nucleation of new spontaneously formed facets and twins, which give rise to a polycrystalline rim. This is also the end of the attempt to use diamond epitaxy on thin substrates with a uniform temperature distribution over the substrate surface [48].

1.2 Using nonflat substrates for diamond homoepitaxy

Since it is apparent that diamond epitaxy occurs both on the upper growth surface of a flat substrate and on the side facets of the substrate, which also interact with the growth medium, we are naturally led to the idea of epitaxial growth of all facets (including side ones) of the seed crystal, resulting in an increase in all dimensions of the crystal. In particular, all surfaces of the substrate should grow in the form of a parallelepiped with polished {100} upper and side facets [49]. Even growth on a diamond anvil was implemented [50].

The growth of a crystal located on a substrate holder shows that the material in the upper part of the substrate grows faster than in the lower part [51]. Apparently, this is due to the difference in key growth parameters along the height of the substrate, primarily with a decrease in the plasma temperature in the downward direction and a decrease in the concentrations of atomic hydrogen and hydrocarbon radicals in it. We emphasize once again that supersaturation during CVD growth is determined not by the ratio of methane and molecular hydrogen concentrations in the gas mixture, but by the ratio of the concentrations of active hydrocarbon radicals (methyl radicals) and atomic hydrogen near the growth surface. The composition of radicals under the microwave plasma conditions currently used (gas mixture pressure greater than 100 mbar, plasma temperature greater than 2600 K) is determined primarily not by electron impacts, but by thermal collisions of particles in the plasma, i.e., by the gas temperature [11, 52]. In this case, even a small change in the gas temperature exponentially alters the concentrations of key growth radicals, and, which is important, according to different laws (see Fig. 3). In the center of the plasma cloud, the proportion of atomic hydrogen relative to molecular hydrogen can reach 60% [53]. As shown by detailed and reliable calculations and the results of measurements of the temperature and composition of the plasma, the latter changes greatly from the center of the plasma ball to its periphery and especially greatly near the substrate [11, 53, 54]. Therefore, in microwave CVD technology, the design of the reactor, the shape of the substrate, its location relative to the plasma cloud, and even the shape of the substrate holder, which determines the configuration of the electromagnetic field near it, are of great importance [55]. This is illustrated by Figs 2 and 3. We consider the inhomogeneity of the plasma by volume to be the main disadvantage of microwave CVD technology.

Figure 1a shows the faceting scheme of our sample in the form of a prism made of a cube with polished facets (001), {311}, and {110}, while Fig. 1b shows a view of the sample after 15 hours of growth. During the crystal growth, new facets of the {100} system, {111} system, and {311} system spontaneously appeared. Also in Fig. 1b, the crystal growth towards the top is visible. This indicates a very strong change in the key growth parameters along the vertical of the sample.

In instructive study [56], the microwave CVD method was used to grow diamond on a $3 \times 3 \times 1$-mm substrate with thoroughly polished {100} facets, located vertically on a substrate holder. Such experiments show that the growth conditions change sharply with height (Fig. 2a). Figure 2b shows the change in the Raman scattering spectra of the grown material along the height of the substrate from top to bottom, and Fig. 2c shows the change in the morphology of the grown materials (according to the scheme in Fig. 2b): from layered monocrystalline growth through polycrystalline, to nanocrystalline, and finally graphite material. As pyrometric measurements show, the crystal temperature decreases from 1050 to 900 °C downwards (Fig. 2a). All of the above clearly indicates that the concentrations of both methyl radicals and, especially strongly, atomic hydrogen decrease downwards, and according to different laws (Fig. 3). This complicates the task of growing crystalline-perfect diamond on the side facets of a nonplanar substrate and, thus, induces specialists to reject this approach. The heterogeneity of the key growth parameters in the case of microwave CVD is illustrated by the modeling of purely hydrogen plasma in Fig. 3a [57]. In hydrogen-methane plasma, such heterogeneity has a very strong effect on the distribution of particles in the plasma (Fig. 3b) [49].

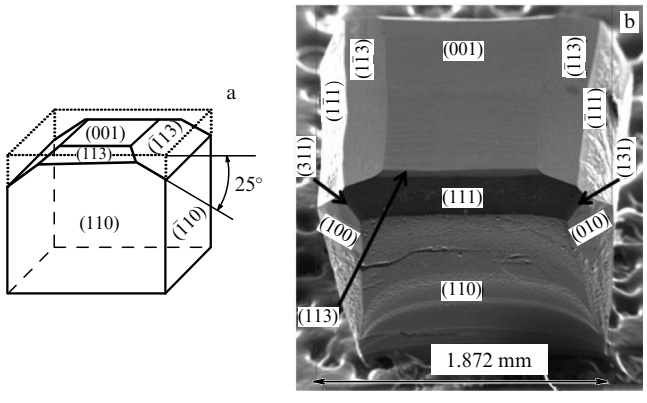

Figure 1. Truncated prism faceted from a cube measuring $1.6 \times 1.6 \times 1.6$ mm according to scheme (a); (b) SEM image after 15 h of growth in a microwave reactor.

Figure 3a shows that, in a wide range of pressures and discharge powers (which must be increased in a coordinated manner so that the size of the plasma cloud does not change), the electron density and plasma temperature in the center of the plasma cloud do not change very significantly. However, due to the exponential temperature dependence of the kinetics of formation of atomic hydrogen, its concentration varies in a wide range. Due to reactions of type (4), it strongly affects the concentration of all particles in the plasma $H_2 + CH_4$ (Fig. 3b), including growth methyl radicals [58]. As can be seen from Fig. 3, near the growth surface, the main plasma parameters differ significantly even in the horizontal plane [59], but they change especially strongly along the vertical axis (Fig. 3b) [60]. Therefore, the position of the substrate relative to the plasma cloud has a great influence on the key growth parameters (concentrations of H and CH_3 radicals, substrate temperature).

In [11], three zones of the plasma cloud were distinguished vertically in a microwave reactor with typical modern growth parameters: (1) the heating and diffusion zone — from 6 to 3–4 cm above the substrate; (2) the atomic hydrogen formation zone (where the gas temperature is above 2600 K and $n_H > 6 \times 10^{15}$ cm^{-3}) — from 3–4 to 0.2–0.5 cm above the substrate; (3) the boundary diffusion layer (< 0.5 cm) with a large energy flux and a strong decrease in the gas temperature and atomic hydrogen concentration (approximately 30 times) downwards toward the substrate. Moreover, according to modeling and actinometric measurements, an increase in the discharge power shifts the maximum of the gas temperature and atomic hydrogen concentration toward the substrate. Adding methane to the gas in a proportion typical of CVD diamond growth (1–7%) does not significantly affect the key plasma parameters.

The growth conditions for the side facets can be made more uniform by placing the substrate on a substrate holder in the form of a truncated pyramid [61]. Another way to reduce the vertical substrate temperature gradient is to reduce heat transfer from the substrate to the substrate holder by, for example, placing a heat separator with low thermal conductivity under the substrate. It is much more difficult to equalize the plasma temperature in the space near the substrate. In this approach, new reactor designs are being

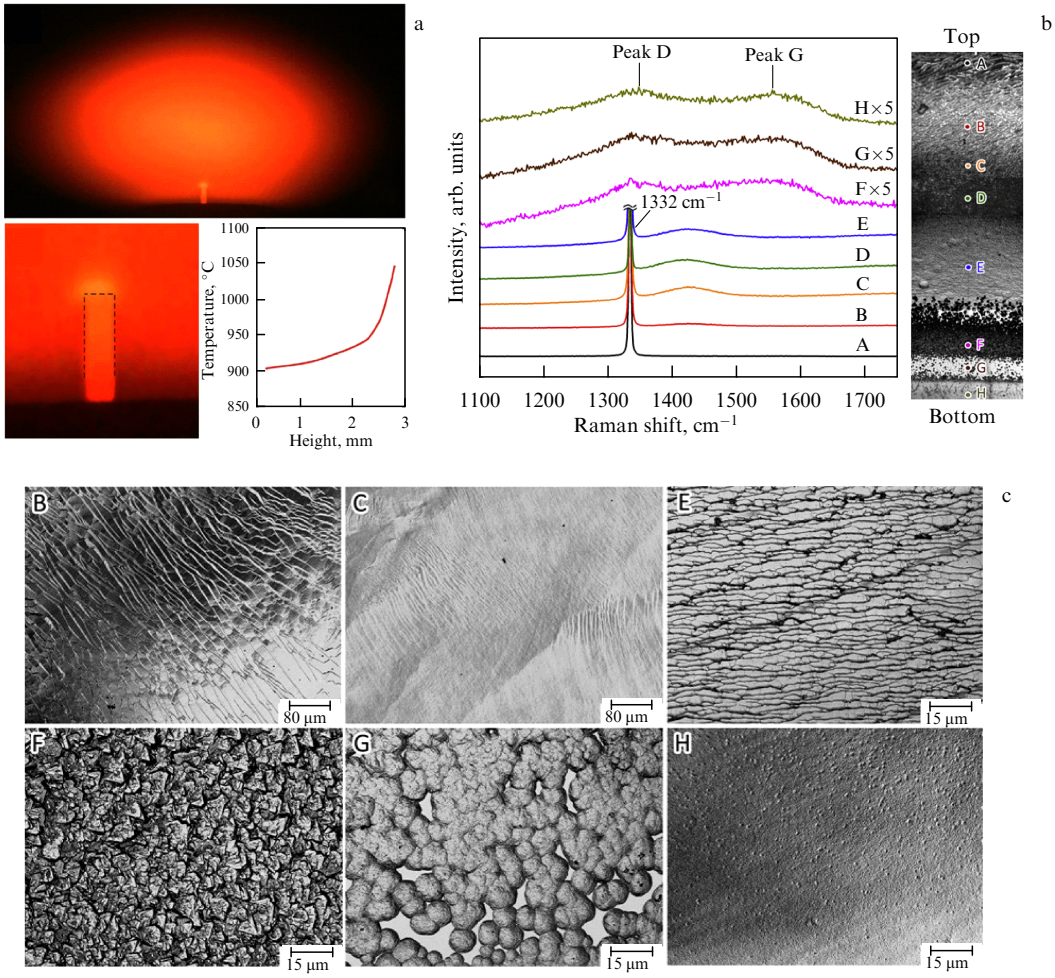

Figure 2. Phenomena occurring during CVD growth of a vertically placed parallelepiped substrate. (a) View of substrate growing in reactor and its temperature change with height. (b) View of material grown on side of substrate and Raman scattering spectra. (c) Morphology of material on side of substrate according to scheme in panel b. (Adapted from [56].)

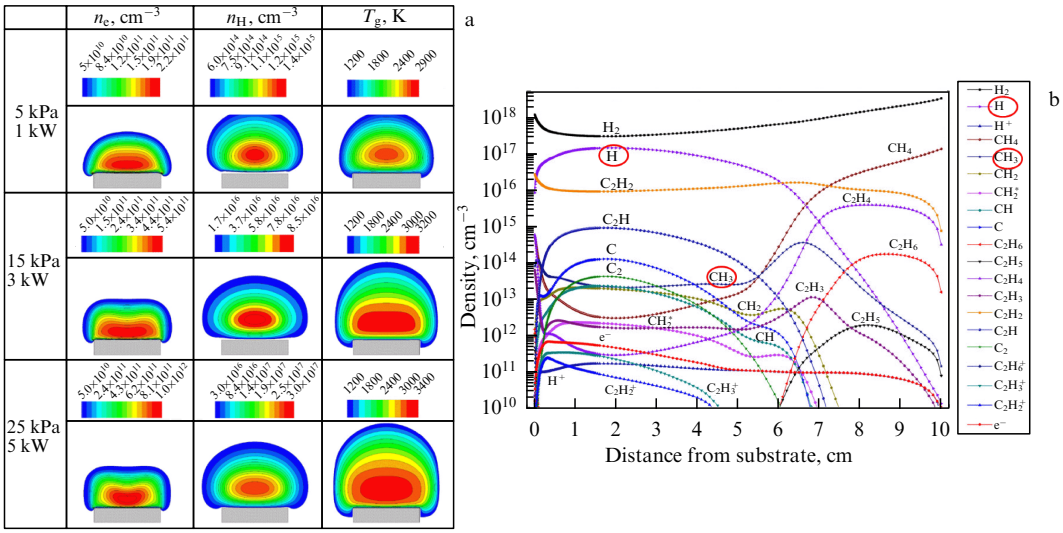

Figure 3. (a) 2D patterns of distributions of key plasma parameters: n_e is electron concentration, n_H is atomic hydrogen concentration, T_g is gas temperature in the plasma. (b) Calculations from 1D modeling of vertical distribution of main particles in hydrogen–methane plasma under the following conditions: pressure of 200 mbar, discharge power of 3 kW, substrate temperature of 850 °C, 4% methane. Main growth radicals H and CH_3 are highlighted.

developed [11, 62] and inert gas additives, such as Ar, are used in the plasma. However, the main way is to increase the discharge power and gas pressure in a coordinated manner. As can be seen from Fig. 3a, this enhances the

plasma homogeneity and the concentration of atomic hydrogen [11].

In [63], heat flows and heating of a diamond substrate in microwave CVD technology were analyzed. It should be taken into account that, at typical epitaxy temperatures, the thermal conductivity of diamond is many times lower than at room temperature. On the other hand, diamond already has its own charge carriers capable of absorbing electromagnetic radiation and maintaining heat transfer. In addition, the diamond substrate is exposed to hard ultraviolet (UV) radiation from the plasma, which should generate nonequilibrium charge carriers in diamond. However, the main source of substrate heating is heat transfer from the hot gas. Heat is removed from the substrate by thermal radiation and heat transfer to a cooled substrate holder. In [48], the horizontal temperature distribution of the (001) growth facet was measured. It turned out that, in the corners of the plates, especially thick ones, the temperature is about 20 degrees higher than in the center of the plate due to the increased microwave field strength and, accordingly, the higher gas temperature near them.

Figure 7 from our study [24] shows phenomena in the process of epitaxial growth of the facets of a small seed crystal with all polished {100} facets. During the growth, the crystal habit changes [64]: the (001) face changes its shape and area and, what is very important, new facets {111}, {110}, {311} spontaneously appear (similar to Fig. 1b). As can be seen from Fig. 1b, the main facets forming the crystal habit in the process of CVD growth are the facets {100}, {111}, {110}, and {311}.

2. Thermodynamic approach to growth of diamond single crystal

Diamond growth using CVD at low gas pressures is quite consistent with the thermodynamic laws of crystal growth in general and diamonds (natural and HPHT) in particular [65, p. 184]. Usually, with reference to the phase diagram of carbon in temperature-pressure coordinates, it is indicated that diamond growth is possible only at high pressures [7]. But, in the case of CVD diamond growth, one more very important coordinate must be added to these two, namely, the concentration of active hydrogen in the gas medium, which, as has become clear over time, performing many functions, shifts the equilibrium in favor of the diamond phase [66].

For CVD diamond, the general law of crystal growth is valid — an increase in the driving force of crystallization $\Delta\mu/kT$ leads to an increase in the growth rate and a deterioration in the crystalline perfection of the growing material. Here, $\Delta\mu$ is the difference between the chemical potentials of the growth phase (in our case, the gas phase) and the growing diamond. Under conditions of a high crystallization driving force, adsorption, normal three-dimensional growth is possible, but in this case a very imperfect material grows (see Fig. 2): a block structure with low-angle boundaries, texture, skeletal and dendritic forms, twins, and then, as supersaturation increases, cuboids with a polycrystalline rim, spherulites (ballases), and polycrystalline intergrowths (carbonado, bort) [65, pp. 167–197].

With regard to diamond growth with the CVD method, the change in crystalline perfection with an increase in the crystallization driving force determined by supersaturation is illustrated by Fig. 3 in [67]. All other things being equal, the diamond growth rate increases monotonically with an increase in the methane concentration $[CH_4]$. At $[CH_4] = 2\%$, the surface of the film with small pits shows competition between growth and etching. At $[CH_4] = 3\%$, layered growth with macrosteps is observed with a film growth rate of 15.6 μm h^{-1}. At $[CH_4] = 4\%$, the relief of the diamond film develops strongly, and mounds and hillocks grow, near the tops of which twin growths appear over time (see Sections 7.4 and 7.5 below). At $[CH_4] = 5\%$, although the growth rate reaches 51 μm h^{-1}, a large number of twins are formed in the growing film, producing polycrystalline regions.

The driving force of crystallization in microwave CVD technology also depends on the location of the substrate relative to the plasma cloud and on the reactor design, which determines the configuration of the electromagnetic field and the ratio of the concentrations of hydrocarbon radicals and atomic hydrogen. Therefore, different authors using the same general growth parameters (substrate temperature, gas pressure, methane fraction, discharge power) realize different degrees of supersaturation of the gas phase and different driving forces of crystallization.

Crystal growth is always a competition between two processes: the incorporation of atoms into the crystal and their removal (desorption, etching) into the growth medium. In the case of diamond growth by the CVD method, two more processes must be added: the growth of the graphite sp^2 phase and its etching. Thus, diamond growth is a competition of four processes, when the rate of growth of the diamond sp^3 phase is higher than the rate of its etching, and the rate of growth of the graphite sp^2 phase is lower than the rate of its etching. The main agent of such relationships is atomic hydrogen, which shifts the thermodynamic potential in favor of diamond growth. High-quality homoepitaxy of crystals, including diamond, is possible only under conditions of a small driving force of crystallization, when the rate of carbon incorporation into the crystal only slightly exceeds the rate of carbon etching [68] and two-dimensional layered growth is realized, sometimes, perhaps, due to screw dislocations, but usually due to the appearance of two-dimensional nuclei (see Section 4.1 and Fig. 5 below). As practice has shown, an increase in supersaturation, naturally, increases the growth rate but also leads to an accelerated development of the relief of the growth surface (001) of diamond, the rapid formation of twin growths [69], and even the precipitation of the graphite sp^2 phase (see Fig. 2).

According to the thermodynamic laws of crystal growth, the equilibrium shape of the crystal is determined by those facets that provide the minimum surface energy of the entire crystal. Usually, they are low-index facets with the lowest density of interatomic bonds in their sections. The habit of diamonds grown from solution (natural and HPHT crystals) is almost entirely determined by the {111} facets, which have minimal surface energy due to the minimal density of interatomic bonds perpendicular to the {111} plane. In CVD technology, saturation with hydrogen (hydrogenation) of the surface of the {100} crystallographic face and its reconstruction according to the (2×1) type [70] reduces its surface energy compared to other facets and brings it closer to the hydrogenated {111} face. As applied to CVD diamond, the thermodynamic approach was developed at the Materials Science Laboratory of the University of Paris 13 (France) based on the analysis of the habit of single crystals grown with different growth parameters [49, 64, 71–73]. The evolution of morphology during crystal growth is determined by the growth rates of the V main low-index crystal facets, namely

{100} and {111}, as well as {110} and {311}. For ease of analysis, dimensionless parameters are introduced that characterize the ratios of the normal growth rates of low-index facets to the growth rate of one of them, namely the {100} face:

$$\alpha = \frac{3^{1/2} V_{100}}{V_{111}}, \quad \beta = \frac{2^{1/2} V_{100}}{V_{110}}, \quad \gamma = \frac{11^{1/2} V_{100}}{V_{311}}. \qquad (9)$$

It is customary to introduce coefficients into the parameters α, β, and γ that characterize the moduli of the corresponding vectors $\langle 111 \rangle$, $\langle 110 \rangle$, and $\langle 311 \rangle$. If one of the parameters is much greater than the other two, the equilibrium shape of the crystal takes the form of one of the plate polyhedra of the octahedron (type {111} facets), the rhombododecahedron (type {110} facets), or the tetragontrioctahedron (type {311} facets). In addition, at different growth stages, polyhedra with different types of facets can form. Figure 9 in [24] shows a diagram of possible equilibrium crystal shapes, depending on the values of the parameters α, β, and γ. Analyses of this diagram and experiments in different growth groups seem to show that long-term growth of cubic crystals formed only by {100} facets is not possible. This key conclusion is discouraging, since the growth of {100} facets has so far produced the highest quality material, both in terms of structural perfection and impurity composition. As shown below, growth due to {111} and {110} facets is extremely undesirable. Analysis also indicates the fundamental possibility of growing a crystal in the shape of a trapezoid (tetragontrioctahedron) formed by {311} facets. In this case, there is hope to delay or even avoid the development of undesirable {111} and {110} facets during the growth process [73].

In [72, 73], the development of the habit of four substrates in the form of flat cylinders with upper facets polished in the {110}, {100}, and {311} planes and with a deviation from the {100} plane by 10° in the [110] direction was simulated. Since the {311} growth facet often forms spontaneously during the growth process and appears promising for long-term diamond epitaxy [74–76], the simulation was performed with growth parameters $\alpha = 1{,}8$, $\beta = 1{,}1$, $\gamma = 4$, corresponding to the ratio of normal facet growth rates $V_{\{110\}} > V_{\{100\}} > V_{\{111\}} > V_{\{311\}}$, i.e., ensuring the dominance of the {311} growth facets. Unfortunately, even under these conditions, as shown by modeling and growth experiments [72, 73], growth facets {111} and {110}, prone to twinning, spontaneously appear along the perimeter of the plate.

In [72, 73], a detailed modeling of the development of the habit of polished substrates of the initial shape in the form of Platonic polyhedra (cube, octahedron, rhombododecahedron, tetragontrioctahedron) with different growth parameters α, β, γ is also performed. Modeling and the practice of epitaxy, unfortunately, again demonstrate the spontaneous formation of new low-index facets (including undesirable {111} and {110}) during epitaxy. However, in reality, due to a strong change in the key growth parameters along the horizontal and especially lateral surfaces of the substrate, the thermodynamic approach is oversimplified.

3. Problems of diamond homoepitaxy using CVD method

Practice has shown that, in the case of a substrate in the form of a (001) plate, during epitaxy on the upper growth facet (001), the surface relief constantly develops due to the appearance of various morphological elements, including a grouping of growth steps with the formation of macrosteps, meandering steps, pointed hillocks, and flat-topped mounds (described in our book [77] in Section 7.3). Sometimes, the growth surface becomes wavy, the growth elements taking the form of 'scales,' 'tiles,' 'dunes,' etc. Due to the convergence of growth layers from different directions, depressions and convexities are formed [78]. As a result of the development of relief, over time, twin growths inevitably form and grow on the growth face (see Figs 27 and 28), and a polycrystalline rim grows on the sides of the plate. Moreover, with absolutely identical growth modes and even in one growth session with several similar substrates, even those made from one crystal, a strong spread of growth results is observed on different plates, both in growth rate and in terms of the morphology of the growth surface [79, 80]. This is explained by the role of the crystallographic orientation of the substrates and their different positions relative to the plasma cloud.

Already in [81], it was discovered how strongly the result of epitaxy depends on the crystallographic orientation of the substrate surface. Great hopes were associated with the precise selection of the vicinal angle (deviation in the growth surface from the crystallographic face (001) by 3–8° [82–87] or more [88, 89]), since, as experience has shown, on a face very close to (001), relief quickly develops, and mounds and hillocks are formed, followed by twins. In general, with an increase in the vicinal angle (of course, up to certain limits [90] (see Section 8), as experience shows, the morphology of homoepitaxial films improves [91, 92]. Attempts have been made to use nonplanar, in particular pyramidal, substrates [93].

Variants of periodic changes in growth conditions [94, 95] and operation in a pulsed mode [16, 96–100] have been tested. Multi-stage recipes using ion implantation [101, 102] and an exotic method of growing by creating an array of needles on the substrate [103] have been proposed. To improve the morphology of the growing film, Ar is added to the gas mixture. This helps to increase the homogeneity and temperature of the plasma due to a decrease in the thermal conductivity of the gas [89, 104–108] and increase the size of the plasma cloud, which allows working at elevated gas pressures [109, 110], providing higher growth rates [111]. However, there is an opinion that in this case some role is played by an uncontrolled admixture of N_2 in Ar, a small addition of which to the gas phase significantly (by orders of magnitude) increases the epitaxy rate. It is also believed that a small addition of oxygen to the gas mixture has a beneficial effect on the morphology of the growing diamond homoepitaxial film [89]. It can be in the form of O_2 [112–114], CO_2 [115, 116], or even alcohol [117]. The addition of boron to the growth medium for growing doped diamond, as practice shows, does not affect the morphology of the growth of epitaxial films on the (001) face. However, all of these measures only allow temporarily delaying the development of the destructive processes described above. The growth of 1–2 mm of epitaxial material in one session on a well-prepared face vicinal to (001) [43] is considered to be an achievement.

The non-uniformity of the substrate surface temperature [45] and the vertical gradient of the substrate temperature during growth [51, 118], which manifests itself in differences in growth conditions along the substrate height (Figs 1b and 2), are considered to be one of the sources of morphological instability in diamond epitaxial growth. The role of non-uniformity of the electromagnetic microwave field, especially

near the substrate corners, is also indicated [45, 119]. Unfortunately, however, all the above-described manifestations of the development of the growth surface morphology are of a general nature and arise during diamond epitaxy using other CVD technologies: in DC plasma [69, 120], during activation of a gas mixture by a hot filament [91, 121], and even from the flame of an oxygen-acetylene torch [122].

Growth layers from different sources of layer growth at the junction points on the growth face yield a structurally imperfect material with a dislocation network due to the inevitable slight mismatch of the parameters and angles of the crystal lattices in different layers [123]. Large-scale defects (primarily dislocations) from morphological imperfections appear in the volume of the epitaxial material, which is manifested in a complex picture of 'tatami'-type bi-refringence. Structural growth defects, on which impurities are concentrated, also detrimentally affect the electrophysical and optical properties of the epitaxial material [95]. Mechanical stress in a sample with the epitaxial film grown on it contributes to the generation of growth defects due to the mismatch of the lattice parameters when growing a low-nitrogen film on a substrate heavily doped with nitrogen [124, 125]. Mechanical stresses also arise due to the horizontal and, especially, vertical temperature gradient of the substrate [118] (Fig. 2a). Sometimes, they become so strong that the film or even the entire crystal cracks.

It has now become clear that the structural perfection of the material is inextricably linked to the achievement of morphologically stable epitaxial growth [39, 126–128]. As shown in [129, 130], an increase in the thickness of the epitaxial film leads to a deviation in some of the dislocations to its periphery, which improves the crystalline perfection of the epitaxial material. This is also the reason why it is so important to achieve long-term morphologically stable CVD growth of diamond.

For commercial purposes, when synthesizing crystals for jewelry applications, a small nitrogen additive is intentionally (and sometimes unintentionally, due to air leakage into the reactor) introduced into the growth gas medium during epitaxy. It acts as a diamond growth accelerator and, as experience has shown, improves the morphology of the growing film in small concentrations [131–135]. With a large nitrogen additive, the material that grows is of an unattractive yellow or even brown color, which is determined not so much by the nitrogen admixture as by growth defects (see Sections 7.4 and 7.5 below). To refine the material, it is necessary to use high-temperature annealing, either in a vacuum or in high-pressure apparatuses (to reduce diamond graphitization) [136–138]. However, even the addition of nitrogen only saves the situation for a short time.

Currently, to grow a significant amount of CVD diamond material on an HPHT substrate, it is necessary to periodically remove it from the reactor, trim the polycrystalline rim along the perimeter, and re-polish the growth surface for a new growth session [139, 140] (see https://www.youtube.com/watch?v=kV7T0vi3rIE). The number of such sessions is sometimes as large as 5 [141]. Such growth interruptions lead to the formation of additional defects in the grown material (including dislocations) and the capture of impurities [32, 142, 143], which is clearly manifested in luminescence (Fig. 7.13 from [77]). In the luminescence pattern, thin lines of blue glow running perpendicular to the surface relate to dislocations, while thick bright lines parallel to the growth surfaces mark forced interruptions between growth cycles. For a long time now, the best single-crystal diamond in terms of purity and crystalline perfection, suitable for electronic applications, has been grown by the CVD method by ElementSix (www.e6cvd.com) [144–146]. However, on the sidewalls of high-quality single-crystal plates of 500-μm thickness sold by the company, at least two of the above-described growth interruptions are clearly visible in the luminescence.

Many problems of CVD technology were recognized 18 years ago [147]. Every year, many dozens of articles devoted to CVD diamond growth are published [27]. However, it must be noted that the progress in CVD technology for epitaxial growth of single-crystal diamond has slowed down recently: long-term morphologically stable epitaxy of the crystal is impossible: surface relief develops (see Figs 12 and 26 below); over time, the appearance of twin growths on the growth surface is inevitable (see Figs 24c, d, 27, 28 below), there is overgrowth with a polycrystalline rim (see Fig. 12 below), and structural perfection of the material is not achieved. Since the publication of good reviews and books [11, 24, 27, 89, 148–158], there has been no fundamental progress in the technology of CVD homoepitaxy of diamond. The great potential of using CVD diamond [89, 159, 160] is still being realized ineffectively. There is a pressing need to overcome these difficulties.

4. Layered growth

The vast experience in homoepitaxial growth of single crystals, including diamonds, shows that good CVD epitaxy occurs exclusively by a layer-by-layer mechanism with a low driving force of crystallization [69, 161–163]. High-resolution measurements by atomic force microscopy (AFM) and scanning tunneling microscopy (STM) also confirm the purely layer-by-layer nature of CVD diamond growth on the {100} and {111} facets [82, 162, 164–167]. In this case, macrosteps that are clearly visible in an optical microscope are often observed, i.e., a grouping of growth steps occurs (see Figs 12, 18 and Section 7.1 below). All further analysis of diamond homoepitaxy by the CVD method is entirely based on the laws of layer-by-layer growth.

The apparent development of layers along the growth face shows that, macroscopically, it is vicinal (Fig. 4). The vicinal angle φ is determined by the ratio of the height of the atomic step a (or macrostep) and the width of the atomically smooth terrace, equal to $a/\tan\varphi$ [168].

If the lateral growth rate of the steps is v, then the normal growth rate of the face V is determined by the formula

$$V = v\tan\varphi\,. \tag{10}$$

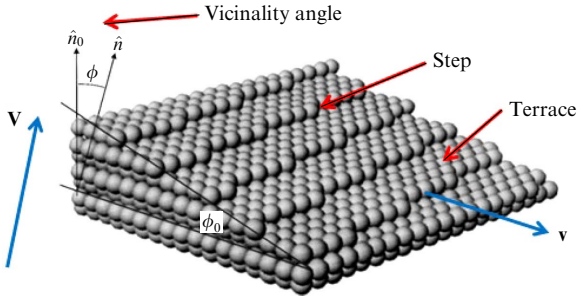

Figure 4. Staircase of growth steps on the vicinal surface.

It should be emphasized now that, for continuous growth in layers to occur (as in Fig. 4 from left to right), the growth layers must originate somewhere. Special attention to this important circumstance is paid below. Equation (10) shows that, for the same lateral velocity of the face v, the smaller the vicinal angle φ, the lower the normal velocity of the face V. According to the law of growth kinetics, the crystal is faceted by the facets of the slowest growth. This implies that, in the process of homoepitaxy of a crystal, there is a tendency for the fast growth facets to wedge out, and its growth facets increasingly approach the low-index slow growth facets (vicinality angle φ decreases), and this is constantly manifested in the practice of diamond homoepitaxy.

4.1 Basic elements of layered growth

Since thermodynamics cannot explain the kinetics of crystal growth, Kossel and Stranski developed a model of layered crystal growth based on the theory of Burton, Cabrera, and Frank (BCF) [169] [65, pp. 38–39]. It is based on the concept of the diffusion of adsorbed atoms (adatoms) along atomically smooth terraces of growth layers (as in Fig. 4) [170]. In this model, an adatom is described as a cube with one chemical bond on each of the six facets of the cube. Such a cube, when it appears on an atomically smooth terrace, forms only one bond with the neighboring atom that is part of the crystal. Because of such a weak bond, the adatom can easily diffuse along the surface of the terrace. In the corner of the growth terrace, two of its bonds are already involved, i.e., such a position is already more stable. It is clear that this is a simplified model and that the carbon atom is not a cube: it has only four directional bonds. In addition, it is not atoms that participate in CVD growth, but hydrocarbon radicals. This notwithstanding, this simple model describes surprisingly well the fundamental features of the processes during layered growth of crystals (even polyatomic ones). Figure 5 shows a model that schematically shows all the main elements and processes on the vicinal face during the growth of a monatomic crystal. In the model displayed in Fig. 5, two atomic terraces (upper and lower) are formed by atoms presented as balls of light gray and dark gray colors, respectively.

The edge of the upper terrace forms a step, which is not necessarily straight — it has kinks. An adatom (more precisely, a hydrocarbon radical) adsorbed from the gas phase (process 1) on an atomically smooth growth terrace is bound to the crystal by the smallest number of bonds (down to one). This is a weak bond, in which the adatom can diffuse along the terrace (process 2), but with high probability it is desorbed (process 3) under the influence of a hydrogen atom from the gas phase in a reaction of type (8). Under conditions of a low driving force of crystallization, crystal growth is characterized by a slow rate (often the excess of adatom incorporation compared to their desorption is less than 0.001).

During the diffusion process, the adatom can manage to get into the corner formed between the lower terrace, along which it diffuses, and the upper terrace (process 4). Due to the greater number of bonds, the position in the corner between the terraces is stronger. Nevertheless, diffusion of an adatom along the step corner (process 5) is still possible, and we present a great deal of evidence of this further on. An adatom that gets into a step bend during such a motion (process 6) has a much stronger bond with the crystal. According to the Kossel and Stranski model, it is only when it gets into a step bend that an adatom becomes part of the growing crystal. On

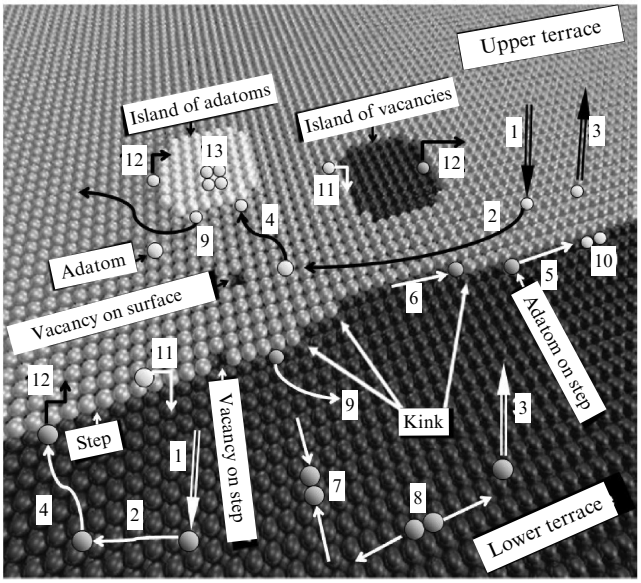

Figure 5. Schematic diagram of main elements and processes on growth vicinal surface in ball model.

a terrace and even in a step corner, it forms an insufficient number of bonds with the crystal and with a high probability will eventually be desorbed into the gas phase. In a random process of diffusion along a terrace, adatoms can combine to form a dimer (process 7). In this case, each atom of the dimer has, on average, more bonds than a single adatom. Therefore, the process of motion of such a dimer is greatly hampered, and is unlikely to be possible at all. However, there is a high probability that such a dimer will disintegrate (process 8). An adatom can also break away from the step corner and again end up alone on the atomic terrace (process 9), from where it will most likely be desorbed into the gas phase. As a result of diffusion along the step corner (process 5), two adatoms can meet and form a strong dimer at the step corner (process 10). For each of the adatoms, this position is equivalent to the position in the step bend (6), and it is then that they become part of the crystal. This is the main mechanism for the development of unevenness of the edge of the growth terrace under conditions of random diffusion processes. It is worth mentioning two more possible processes that are discussed below: the descent of an adatom from the upper terrace to the lower one (process 11) and the ascent from the lower terrace to the upper one (process 12).

During the growth of the upper terrace layer (especially the meandering one, with large bends in the step), a situation is possible when two 'tongues' of the growth layer come close to each other (see below, Section 7.2), leaving behind an unovergrown area, shown in Fig. 5, which is called a vacancy island. If other adatoms manage to join the dimer of adatoms (7), the formation of the two-dimensional island of adatoms shown in Fig. 5 is possible. Just as in the 3D case, here, thermodynamics point to the role of the critical size of the nucleation center [171, pp. 572–574]. If the size of the island of adatoms is smaller than the critical one, with a very high probability, it, like the dimer 8, will disintegrate into individual adatoms. It is only when a 2D island of adatoms of a size larger than the critical one is accidentally formed that, with a high probability, it will grow, and only then does it act as a stable source of growth of a new growth layer or the formation of a mound (process 13). It is clear that, with an

increase in the driving force of crystallization, the probability of the formation of 2D islands larger than the critical size increases. The main factor determining the growth of terraces or the formation of 2D islands is the ratio of the average diffusion length of adatoms along an atomic terrace (process 2) and its width $a/\tan\varphi$.

The model presented in Fig. 5 does not take into account the possibility of adsorption of C_xH_y radicals with $x \geqslant 2$ on the terrace, the content of which in the gas phase can be significant [172] (Fig. 3b). In [173], it was shown that the composition of the C_xH_y radicals should affect the mechanism of layered diamond growth, although the main growth radical is still considered to be the methyl radical CH_3 [174].

As shown below, all the processes displayed in Fig. 5 and described above determine the homoepitaxial growth of diamond by the CVD method. Each of the acts in Fig. 5 is either accompanied by overcoming an energy barrier (for example, diffusion 2 or processes 11 and 12 of descent from a step and ascent to it), or is either endothermic (processes 3, 8, 9, 11, and 12) or exothermic (processes 1, 4, 5, 6, 7, and 10) [175, 176]. All of them are random. The randomness of all elementary acts of the growth process turns out to be one of the sources of morphological instability of crystal epitaxy in general and diamond in particular.

It should be emphasized once again that, in the case of CVD growth of diamond, the processes shown in Fig. 5 involve not carbon atoms, but hydrocarbon monoradicals CH_3, CH_2, etc. Desorption of the adatom (process 3 in Fig. 5) occurs not as a result of evaporation, but as a result of a chemical reaction with atomic hydrogen from the gas phase (in reaction (8)). The surface itself of the growth terrace of the {100} face itself is hydrogenated [174, 177]. During hydrogenation, the {100} face becomes reconstructed according to the (2×1) type (as can be seen in Figs 16b and 19a) [177–179].

The main processes during layer-by-layer growth (see Fig. 5) on the {100} face and partly on the {111} face have been well calculated and modeled:

— adsorption and desorption of hydrogen and methyl radical (processes 1 and 3) [180–190];

— adatom diffusion along the terrace (process 2) [180, 185, 187–194];

— desorption of an adatom from a terrace (process 3) [186];

— attachment of an adatom to a corner of a growth terrace (process 4) [173, 180];

— diffusion of an adatom along a corner of a growth terrace (process 5) [191, 193];

— formation of an adatom dimer (process 7) [186, 188, 189, 194];

— decay of an adatom dimer (process 8) [180, 186];

— descent of an adatom from the upper terrace to the lower one (process 11) [194];

— formation of mounds (process 13) [194].

As can be seen from the diagram in Fig. 5, the area of the upper terrace is always smaller than the lower one, since its growth is fed by adatoms coming along the lower terrace to the corner of the step. Therefore, ELO cannot occur due to the upper terrace overhanging the lower one in the form of a cornice. In reality, ELO occurs due to the growth of lateral facets (Fig. 1b).

4.2 Layered growth on low-index facets

As numerous observations of diamond growth using the CVD method show, only two low-index facets grow by the mechanism of true layered growth: {111} and {100} [195–198], while the remaining macroscopically observed facets are formed by a combination of {111} and {100} layers [195, 199].

4.2.1 Growth by {111} layers. Natural and HPHT diamonds grow from solutions under conditions of a very low crystallization driving force and, accordingly, very low growth rates. Although their habits may differ significantly, they grow predominantly in {111} layers. CVD diamond growth is also often realized in {111} layers, especially in polycrystalline films. Unfortunately, the {111} facet is an easy twinning facet [35], and attempts to enhance the growth rate by increasing the crystallization driving force inevitably lead to multiple twinning and failure of epitaxy. This is clearly seen in optical images and photoluminescence patterns of CVD films grown on the {111} facet under different conditions [200]. *Twinning is the main enemy of diamond epitaxy*.

It is believed that slow epitaxial growth on the {111} face without twins is only possible at a very low crystallization driving force: at temperatures no higher than 900 °C, with a low methane fraction (less than 1%), and without nitrogen additives [201–205]. Thin layers (up to several micrometers) {111} are suitable for the fabrication of vertical semiconductor structures [205]. However, in most applications, the appearance of {111} facets, which are fraught with twinning, should be avoided by any means in the CVD epitaxy process.

4.2.2 Growth by {100} layers. On the main growth face (001) in the CVD technology, a wide range of morphological relief elements is observed during epitaxy: slightly wavy steps (Fig. 12b), 'tiles' (Fig. 12a), 'dunes,' 'scales,' pointed 'hillocks' (Fig. 26a), flat-topped 'mounds' (Figs 26b, c and 27a), and finally, a staircase of macrosteps (Figs 7c and 19b), etc. However, all of them clearly exhibit a layered growth mechanism, namely by (001) layers [206, 207]. At a very low driving force of crystallization, even growth by atomically smooth steps is possible [83, 208]. But macrosteps are observed most often.

4.2.3 Growth of the {110} facet. The {110} facet does not grow in layers independently, although it sometimes forms spontaneously during growth (Fig. 1b). It grows in pyramids formed by the {111} and {100} layers (Fig. 6a). It cannot be used for homoepitaxy due to twinning on the {111} layers (Fig. 6b).

4.2.4 Growth of the {311} facet. Theoretical calculations show that the hydrogenated and reconstructed $C(311)-(2\times1):H$ facet (Fig. 7b) is energetically more favorable than even the

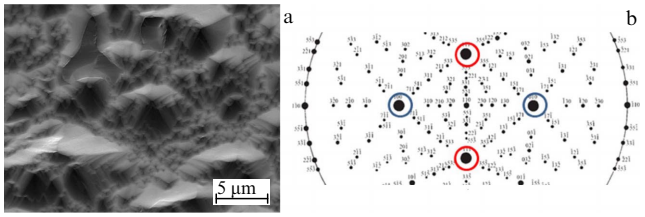

Figure 6. (a) X-ray diffraction image of (110) facet of the sample shown in Fig. 5b after 15 h of growth. (b) Part of stereographic projection in the (110) plane. Marked with red circles are nearest {111} planes, and with blue circles, {100} planes, which together form growth pyramids on {110} facet.

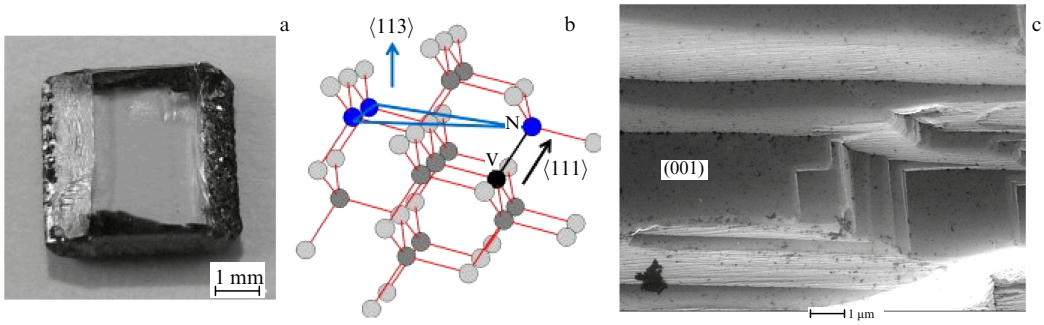

Figure 7. (a) Image of grown diamond film with (113) facet on left side of substrate (rougher). (b) Model of hydrogenated (113) diamond facet. (c) SEM image of (113) diamond facet after 20 h of growth on sample shown in Fig. 1.

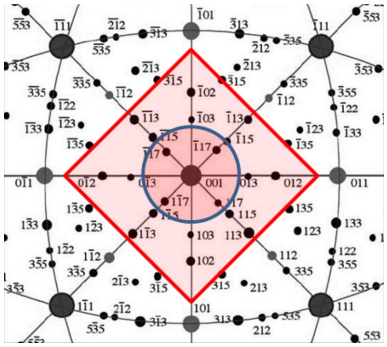

Figure 8. Stereographic projection of (001) facet with regions of possible homoepitaxy. Blue circle in center of projection is discussed below in Section 8.

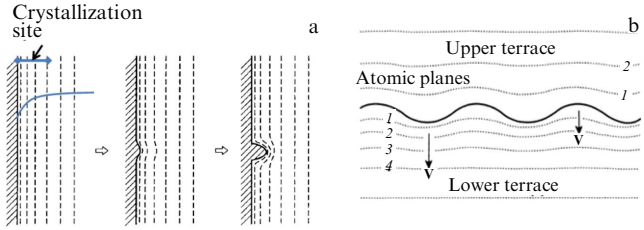

Figure 9. (a) Boundary diffusion layer in three-dimensional case; dashed lines are lines of equal concentration of growth radicals and morphological instability of crystal growth due to boundary diffusion layer. (b) Nature of boundary diffusion layer near edge of growth terrace in two-dimensional case of layer-by-layer growth.

C(100)−(2 × 1):H facet [209, 210]. However, experimental evidence for such a reconstruction is still unavailable. Nonetheless, this is unimportant, since Fig. 7c clearly shows that the {311} facets actually grow in {100} type layers. This is good compared to the {110} facets, which grow as a combination of {100} and {111} layers (see Section 4.2.3). It remains unclear why it is the macroscopic {311} facets that exhibit stable growth (Fig. 7a) and even spontaneously appear during growth (Fig. 1b). For stable growth, the {311} facet requires $\gamma \gg (\alpha, \beta)$, which, according to the data in [73, 211], corresponds to an increased growth temperature and a higher proportion of methane in the gas mixture.

4.3 Facets of growth without twinning

The risk of twinning determines the set of facets suitable for epitaxial growth. Most importantly, they must be located away from the {111} facets of layered growth. In the stereographic projection of Fig. 8, the red square with pink filling highlights the supposed region of permissible angular deviations of the growth surface from the crystallographic facets {100} to ensure layered growth along these facets and to prevent growth in layers {111} — it is precisely the square of this color that is used to emphasize the particular hazard of deviation in the directions ⟨111⟩.

5. Diffusion boundary layer

The most important concept in the physicochemistry of crystal growth from solutions and the gas phase (the case of CVD diamond growth) is the diffusion boundary layer, or diffusion zone. The diffusion zone of crystallization is the boundary zone of the growth medium near the growing crystal, from which atoms for crystal growth are supplied (Fig. 9). Since some of the atoms from the growth medium are spent on crystal growth, it is clear that in the boundary layer near the surface of the growing crystal there is a gradient of their concentration, shown in Fig. 9a, b by dashed and dotted lines. The role of the boundary diffusion layer is significant in the 3D case of crystal growth, but is especially important in the 2D case of layered crystal growth on atomically smooth facets (see Section 7.2) [212].

Associated with the boundary diffusion layer is one of the sources of morphological instability of crystal growth as illustrated in Fig. 9. If, due to the random nature of the processes during crystal growth, a protrusion is formed on its surface (in the 3D case, in Fig. 9a) or on the edge of the atomic layer (in the 2D case, process 10 in Figs 5 and 9b), then, unlike the adjacent crystalline material, such a protrusion turns out to be in a more advantageous position from the point of view of feeding by growth radicals — the angular sector of the boundary diffusion layer feeding this protrusion is larger than in other places. As a result, the protrusion begins to grow at an accelerated rate (Fig. 9a, from left to right). This positive feedback maintains an increase in the surface roughness of the growing crystal, and, with a strong driving force of crystallization, it provides skeletal and dendritic growth of the crystal [65, pp. 27, 28, 47–52]. In the 2D case (sometimes called the Bales–Zangwill instability), the increased angular sector of the supply of the protrusion at the edge of the growth terrace (due to process 4 in Fig. 5) ensures its constant increase (Fig. 9b), which leads to meandering of the steps (see Section 7.2 below). It is counteracted by the process of diffusion of adatoms along the angle of the growth step (process 5 in Fig. 5).

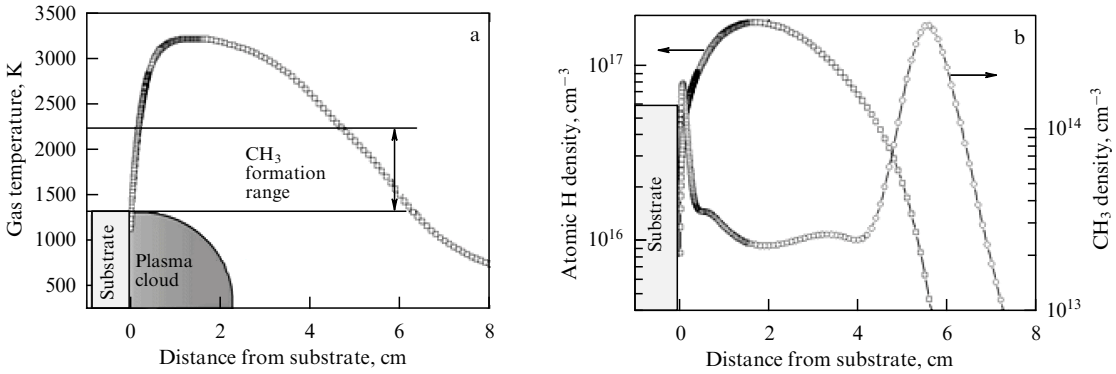

Figure 10. (a) Calculated gas mixture temperature in one-dimensional model at microwave power density of 100 W cm^{-3}, 4% CH_4/H_2, and substrate temperature of 1100 K. (b) Calculated concentrations of H and CH_3 radicals.

However, in the case of microwave CVD diamond growth, another source is much more significant: the concentration gradient of methyl radicals CH_3 and atomic hydrogen H [213–215] in the boundary diffusion layer due to the gas temperature gradient near the substrate (Fig. 10a).

The point is that a high concentration of methyl radicals CH_3 is achieved in the plasma temperature range of 1300–2250 K with a maximum at 1650 K (see Fig. 10). At higher temperatures, CH_3 decomposes to form hydrocarbon radicals with a smaller number of hydrogen atoms (Fig. 3b): CH_2, CH, C, C_2, C_2H_2, C_2H, etc. Since the gas temperature is significantly higher than the substrate temperature, a negative concentration gradient of the CH_3 growth radical (and other hydrocarbon radicals) and atomic hydrogen H arises due to the large negative temperature gradient of the gas in the direction of the substrate (see Section 1.2, Figs 3 and 10b). This is confirmed by direct measurements of the gas temperature near the substrate [106]) and the distribution of methyl radicals [215, 216]. After all, the substrate is heated mainly due to heat transfer from the gas, as shown by experiments with different relative positions of the plasma cloud and the substrate [109]. According to one-dimensional [214] and two-dimensional [217] modeling and measurements [218], the boundary layer near the substrate extends from 1000 to 200 μm at gas pressures from 50 to 300 mbar. As can be seen in Fig. 10b, the methyl radical concentration within this layer decreases by an order of magnitude. Because of such a large gradient, the protruding regions of the growing film are more actively supplied with methyl radicals and grow faster. Thus, a strong positive feedback arises, promoting accelerated growth of the protruding regions of the substrate, which enhances the roughness of the growing surface. This is another, and undoubtedly a very strong, source of morphological instability of CVD epitaxy of diamond.

Given this situation, the substantial change in the driving force of crystallization shown in Fig. 2 depending on the substrate shape and the local temperature on it becomes understandable. In the case of microwave CVD growth of a single crystal, it also indicates the inappropriateness of the thermodynamic approach presented in Section 2 and used in [49, 64, 71–73] to describe the habit of a growing single crystal based on the growth parameters α, β, and γ. This approach was initially developed to analyze the habit of crystallites of polycrystalline CVD diamond films grown by the hot filament method [196, 219, 220], with good homogeneity of the boundary diffusion layer along the film surface. However, when growing a single crystal by microwave CVD, as shown above, the key growth parameters differ greatly even within one growth facet, and especially greatly on its different facets (horizontal, inclined, perpendicular), bordering on regions of the plasma cloud with different temperatures.

Within the boundary layer, the concentration of atomic hydrogen (see Section 1.2 and Fig. 10b) [221], which is the key agent of CVD diamond growth, decreases especially strongly. It is for this reason that the morphology of the material changes so significantly along the height of the substrate in Fig. 2, up to the deposition of sp^2 graphite-like carbon, which, as shown in [222], occurs with a deficiency of atomic hydrogen. In [119], the electromagnetic microwave field was calculated near a substrate in the form of conventional flat plates located on substrate holders of different shapes. In the boundary gas layer near the edges, and especially the corners of the plate, as expected, the electromagnetic field strength is increased. This causes an increase in the substrate temperature in the indicated places [45] and an increased concentration of atomic hydrogen and methyl radicals in the gas phase near them, which implies that, even near the horizontal upper edge of the substrate in the form of a flat plate (in its center, near the edges and corners), both the boundary layer and the degree of supersaturation, and especially the driving force of crystallization, are non-uniform. The effect of positive feedback is additionally enhanced by the superlinear dependence of the crystal growth rate on the driving force of crystallization [65, p. 52]. As a result, as can be seen from the growth morphology in Fig. 12, the driving force of crystallization and the growth rate are significantly higher near the edges and corners of the plate than in its center. This has a fundamental effect on the morphology of the epitaxial material.

As the crystal grows, its growth surface moves to a hotter region of the plasma cloud, which, due to the small thickness of the boundary diffusion layer, leads to an undesirable gradual change in the growth conditions and, consequently, instability of the epitaxy mechanism. An efficient way to combat this phenomenon is to use a moving substrate holder. In the absence of movement, it is necessary to adjust the substrate temperature by changing the discharge power or gas pressure.

6. Regularities of diamond epitaxy in using CVD method

We now describe several important experimental regularities of crystal growth that appear during the growth of single-crystal diamonds when using the CVD method.

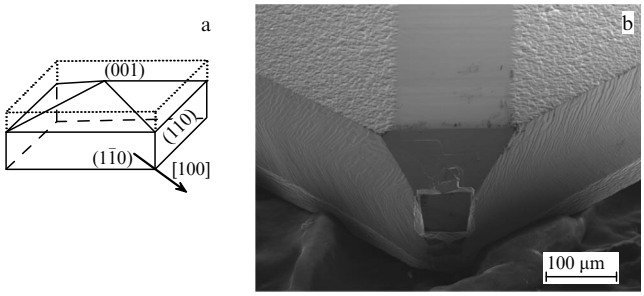

Figure 11. Substrate faceted according to scheme (a) with a 5° deviation angle of upper facets from the (001) plane, (b) after 5 h of growth in microwave reactor with the addition of nitrogen. SEM image: all facets grow, including side ones. Smooth material grows from four upper edges. Formation of a new facet (100) at the corner is visible.

6.1 All-round growth

As noted above, all substrate facets grow, including the side ones (see Figs 1 and 11) [223], of course, with the exception of the face on the substrate holder. It should be taken into account that the growth conditions near the edges and corners of the substrate and along the side facets differ greatly (see Figs 1 and 2). As experience shows, even the inclination of the side facets is of great importance, which can be less than 90° (Figs 1b and 13a) or more than 90° (Figs 1b and 11).

6.2 Spontaneous formation of new growth facets

Figure 1b shows the appearance of new facets of the {100} system: ((100), (010), ($\bar{1}$00), (0$\bar{1}$0)), the {111} system: ((111), ($\bar{1}$11), ($\bar{1}\bar{1}$1), (1$\bar{1}$1)), and the {311} system: ((311), (131), etc.). Figure 11b shows once again the spontaneous formation of the {100} face. Apparently, from the thermodynamic point of view, all of the listed facets are energetically the most favorable under CVD diamond growth conditions. Because of the spontaneous appearance of {100} facets, this picture seriously contradicts the thermodynamic approach developed in [49, 64, 71–73] (see Section 2) as does the growth of polycrystalline films with {100} crystallites [224]. The {100} facets that spontaneously appear on the lateral edges apparently have a very small vicinal angle. As can be seen in Fig. 1b, this leads to the rapid appearance of twin growths on them by the mechanism substantiated further in Section 7.4. It is only in this sense that {100} facets are not stable growth facets, which is discussed below.

6.3 Sources of layered growth

Layered growth originates from growth sources. Specialists in diamond growth by the CVD method pay little attention to this circumstance. However, it is literally apparent (Fig. 12). It is evident from many images presented in many publications that on the (001) facet growth begins from the edges of the plate [45, 67, 225] and from the edges of the crystal (see Figs 1 and 12), converging toward the facet center [44]. The sources of layered growth are clearly visible even at the edges (edges and corners) of the crystallites of the polycrystalline film [226, 227]. It is the growth from the plate edges that provides the characteristic skeletal, concave shape of the main growth surface (001) on standard substrates [39]. In exactly the same way, growth in {111} layers also originates from the edges of the plate. Figure 12a shows that numerous sources of layered growth spontaneously form far from the growth layers extending from the edges, giving a growth relief in the form of 'dunes' or 'tiles.'

This pattern is explained by the role of the boundary diffusion layer. It should be recalled that homoepitaxy of a crystal occurs at a low driving force of crystallization, when the rate of incorporation of atoms into the crystal only slightly exceeds the rate of their desorption. Under such conditions, a great advantage is gained by regions with an increased supply of growth radicals, fed from an increased angular sector of the boundary layer, i.e., regions with an increased driving force of crystallization. The edges and corners of the plate are precisely such places. In addition, the local gas temperature, as well as the concentrations of the main growth radicals near them, are higher, which also increases supersaturation, although, on the other hand, the temperature of the plate itself at the edges is slightly higher than in the center [48]. The increased driving force of crystallization at the edges of the plate leads, in fact, to obvious manifestations of skeletal growth (Fig. 12b) and often even to a breakdown into polycrystalline growth (Fig. 12c), in full accordance with the thermodynamic laws of crystal growth (see Section 2). This is the Berg effect, well known in the physicochemistry of crystal growth [65, p. 49]: at high supersaturations, a new growth layer is formed at the corners and edges before the previous one spreads over the entire surface of the face, which leads to the formation of edge and apical skeletal growths. Skeletal growth is often observed in synthetic HPHT crystals grown under high supersaturation [228, pp. 158–161]. To minimize the Berg effect, it is necessary to achieve as uniform a driving force of crystallization as possible over the entire surface of the substrate. The use of nonflat, pyramidal substrates is a way to solve this problem.

Since the edges of a conventional substrate with unpolished side facets are microscopically jagged, the sources of layered growth on them are individual protrusions, which is

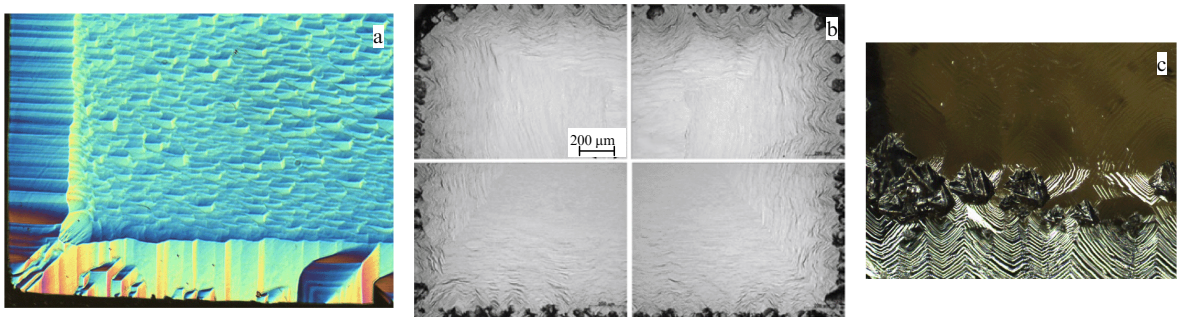

Figure 12. (a) Optical image with differential interference contrast of (001) plate after 10 h of CVD growth. Horizontal frame size is 1 mm. (b) Image of four corners of CVD plate. (c) Enlarged optical image of plate edge with sources of layered growth and twin growths on them. Horizontal frame size is 500 μm.

clearly visible in Fig. 12 b, c. In the center of the plate, there is a convergence of growth layers from numerous randomly formed sources of layered growth on the edges of the plate [229] (Fig. 12a), which negatively affects the crystalline perfection of the material grown. Usually, the most intense growth layers originate from two or three edges. This is explained by the vicinality of the plates: the original substrates are polished so that the crystallographic vector [001] of the plates is deflected towards the edges, where they end up at the top of the staircase of growth steps.

On a substrate faceted in the form of a pyramid (Fig. 11a), in place of the four upper edges of the pyramid, a relatively smooth material grows (Fig. 11b). The width of the stripes of smooth material increases as it grows. Analysis of the topography of this material using optical interference profilometry showed that the sources of layered growth are two parallel lines separating the smooth material and the growth regions with hillocks. The growth layers originating from them converge at the site of the former edge: a groove with an angle of about 179° is formed in the cross section of the smooth material. It is appropriate to call such sources of layered growth linear. On this pyramidal substrate there is also an artificial point growth source in the form of the top of the pyramid. Epitaxy practice has shown that smooth material close to the crystallographic facet (001) quickly grows around it, which, due to the morphological instability of this facet, provokes the formation and growth of mounds on it (see below Section 7.4 and Fig. 26). Therefore, the authors give preference to artificial, linear sources of layered growth.

Other uncontrolled sources of growth layers are scratches and polishing defects of the plate. It is clear that, microscopically, the edges of these scratches also have the appearance of ribs, on which both {100} and, unfortunately, {111} growth layers can nucleate. The combination of such layers produces a complex relief of the material grown on a scratch and can even lead to the rapid appearance of twins [225, 230].

This implies the need for high-quality polishing of the substrates and their careful preparation for epitaxy [231–233], which, however, is a prerequisite for the technology of homoepitaxy of all crystals. Otherwise, the crystalline perfection of the material is low and epitaxy can even break down into polycrystalline growth (Fig. 13).

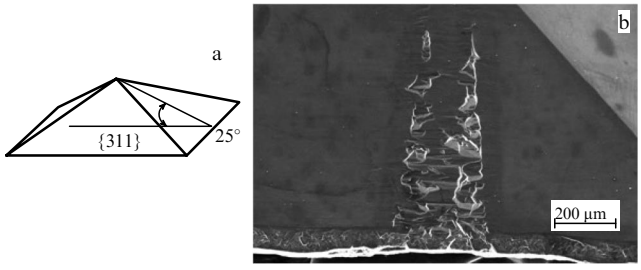

Figure 13. (a) Substrate faceted in the form of a pyramid with polished {311} facets. (b) SEM image. Material grown on a vertical scratch of a poorly polished {311} diamond facet after 10 h of growth.

We emphasize once again that the immense experience of epitaxial growth of many crystals indicates the need for careful polishing and preparation of the substrate for epitaxy [231, 234]. Despite numerous proposals to use ion-plasma etching and chemical-mechanical polishing [235], unfortunately, a technological procedure for preparing the surface of a diamond substrate for homoepitaxy, which would guarantee defect-free nucleation and development of a homoepitaxial layer, has not yet been documented (although it may be used as *know-how*). It is clear that the material grown in place of polishing defects is crystalline imperfect [236] and, at a minimum, contains many defects (Figs 13b, 14 and Fig. 7.12 in [77]).

A defect or impurity on the substrate surface can cause the immediate formation of a stacking fault limited by twin planes, according to the mechanism shown in Fig. 14a. The mismatch of the lattice parameters of the substrate and epitaxial material leads to the emergence of mechanical stresses in the crystal, the formation of misfit dislocations, and the development of dislocation loops (Fig. 14b) [237]. In addition, the authors consider the vertical temperature gradient of the substrate ([118] and Fig. 2a) to be an important source of mechanical stresses in epitaxial diamond, which sometimes even leads to the formation of cracks in the epitaxial film.

6.4 Spontaneous and artificial sources of layered growth

On smooth facets far from the edges, due to the random formation of a cluster of adatoms on an atomically smooth

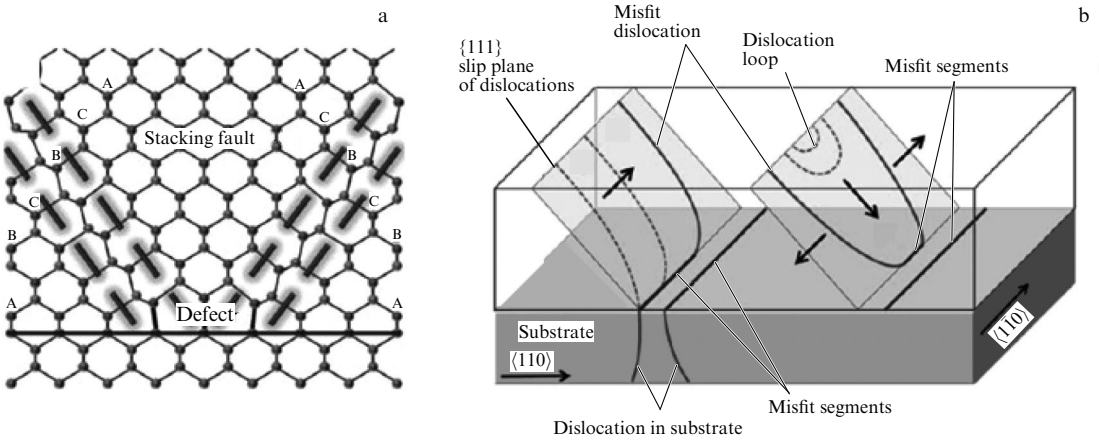

Figure 14. (a) Formation of a stacking fault in homoepitaxial film from a defect on the substrate. (b) Mechanism of dislocation growth from substrate and formation of new dislocations due to mismatch of crystal lattice parameters of the substrate and film.

terrace (process 13 in Fig. 5), a protrusion (a hillock with a sharp top or a mound with a flat top) can form over time, which then, due to increased nutrition by growth radicals (see Section 5), becomes a self-reproducing source of layered growth (the mechanism of formation and growth of mounds is described in Section 7.4). Each of these spontaneous sources produces layers in all directions, which forms morphological elements of various shapes on the (001) face: 'dunes,' 'scales,' 'tiles' (Figs 11b and 12a), hillocks, mounds, etc. The closure of growth layers from them forms a constantly developing relief of the growth surface and provokes the formation of many dislocations [238]. An increase in the relief on the (001) growth facet and an increase in the slope of individual sections of the growth surface are fraught with the spontaneous formation of {111} growth layers (Figs 18b and 27a), which will inevitably begin to twin, leading to a failure of epitaxy (see Section 7.5).

By now, it has become clear that controlled sources of layered growth are needed for good homoepitaxy of diamond. From the abstract of and figures in [239], it is clear that the authors, in fact, created artificial sources of layered growth in the form of ribs on flat substrates by polishing chamfers with deviations from the (001) face by 0.8–11.3°. The authors show that, at a small vicinality angle, the width of the atomic growth terraces becomes so large (see Fig. 4) that uncontrolled 2D sources of layered growth spontaneously arise on it (see Section 7.4). Similar controlled linear growth sources in the form of four ribs on the upper surface of the substrate were obtained on our substrate in Fig. 11a. During the growth process, they yield a smooth epitaxial material (Fig. 11b).

6.5 Staircase of growth steps

Growth on the vicinal face occurs by developing a staircase of atomic steps (see Fig. 4): the edge of each step grows due to the addition of adatoms (processes 6 and 10 in Fig. 5) from the lower terrace. Thus, homoepitaxial growth requires the formation of a staircase of growth steps. However, the original polished facet vicinal to (001) has a roughness determined by grinding/polishing grooves (see Fig. 17) and, of course, does not form such a staircase of atomic growth steps. As a result, at the initial stage, crystal growth occurs mainly from the edges of the sample and usually produces a clearly visible rim of wavy material spreading from the edges to the center (Figs 12a and 15a). The rim is also clearly visible during homoepitaxy on the {111} facet [200]. At the same time, staircases of growth steps are formed.

All of the above clearly indicates the role of the sources of layered growth at the edges of the sample. At a small vicinal angle, a rim develops from all four edges (Fig. 12b). At a vicinal angle greater than 2–3°, the rim originates from two or three edges (Fig. 12a). This clearly determines the direction of the stair of growth steps developing from the edges. Thus, in Fig. 15a, the upper step of the staircase is on the left edge and, as a result, the staircase of growth steps spreads from left to right. Due to imperfect polishing, the left edge turns out to be jagged, so individual protrusions emerge on it, from which predominant growth occurs, in exactly the same way as growth occurs from protrusions on the edges of a conventional plate-shaped substrate (Fig. 12b, c). No growth occurs at all from the right edge on the (001) facet (Fig. 15a), because it turns out to be at the bottom of the growth step staircase. The upper and lower edges also provide layered growth. Figure 15b schematically shows how this process can occur due to the diffusion of adatoms along the atomic terraces of the forming growth step ladder. The (001) facet displayed in Fig. 15a is bordered by polished {311} facets (Fig. 2a), which also grow, leading to an increase in the lateral dimensions of the upper part of the sample (Fig. 2b). It is this type of growth that provides ELO. In Fig. 15a, this is exhibited on the left edge in the spread of growth layers also to the left, up to the boundary with the {311} face. The layered growth mechanism completely rules out the possibility of ELO due to the overhang of the upper layers over the lower ones in the form of a cornice.

If the understanding of the role of the increased angular sector of the boundary diffusion layer near the source of layered growth (edge, vertex) is correct, it is natural to assume the reason for the generation of new growth steps on such a source. It consists in the increased probability of formation of a 2D island of adatoms on the terrace (process 13 in Fig. 5). Due to the enhanced supply of adatoms, such an island grows into a new growth terrace. The rate of generation of new growth terraces can be appropriately called source power I, equal to the number of generated growth terraces per unit time. It is clear that, in addition to the angular sector of the boundary diffusion layer, it also depends on the supersaturation of the gas near the source. The development of a face from the source of layered growth is determined by the ratio of the rate of formation of new growth steps on source I and the rate of propagation of growth layers v along the face. If the source power is less than the rate of propagation of the steps ($I < (v \tan \varphi)/a$, where a is the height of the growth layer), the growth terraces quickly reach the edge of the face.

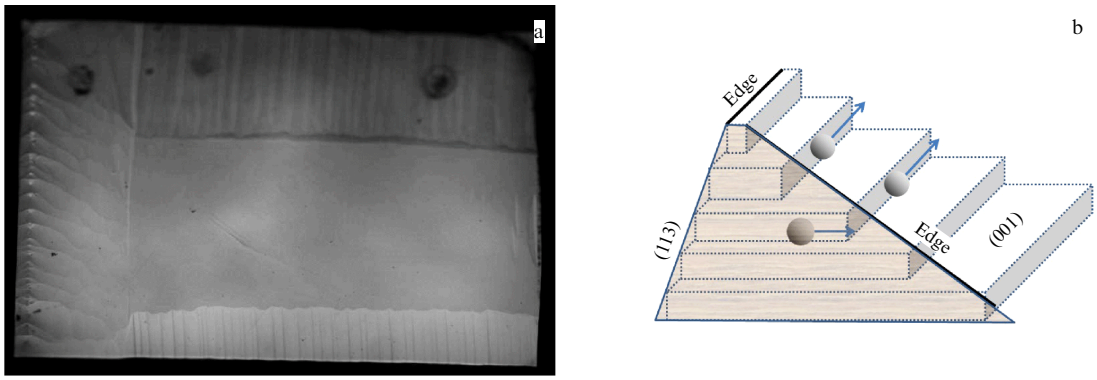

Figure 15. (a) Upper facet of a sample cut according to scheme shown in Fig. 2a after 5 h of growth. (b) Schematic diagram of development of a staircase of steps on lower edge of this sample.

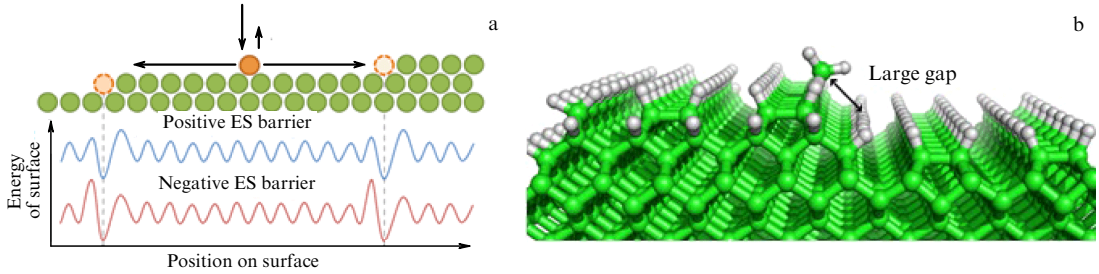

Figure 16. (a) Schematic diagram of the effect of ES barrier on layered crystal growth, (b) Physical cause of ES barrier on hydrogenated (001) diamond facet.

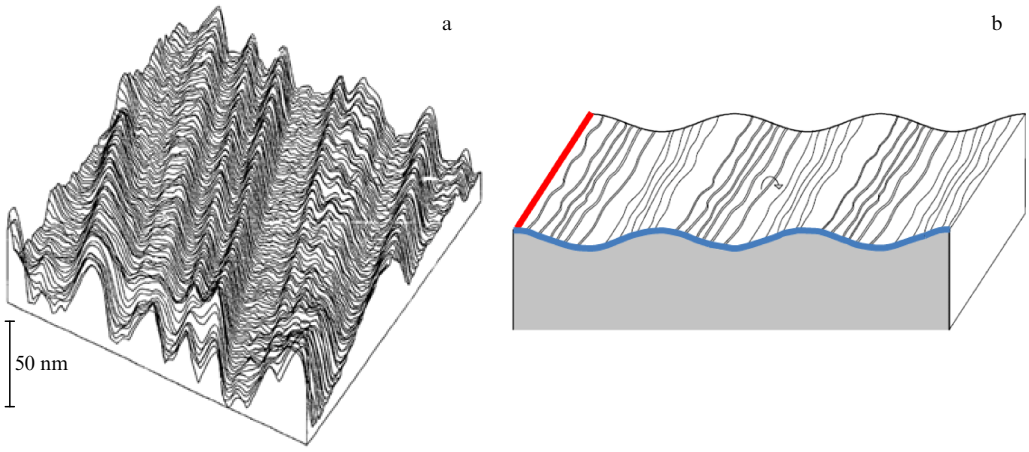

Figure 17. (a) STM topography of {100} diamond facet polished in soft direction. Image size in plan is 500 × 500 nm. (b) Schematic representation of atomic terraces on a wavy polished diamond surface.

This results in the growth facet gradually approaching (001) (vicinal angle φ decreases [129]), which, as shown below, is an adverse factor. This is exactly what happened with the substrate in Fig. 11a, which provoked morphological instability in the form of mound formation (Fig. 26). If, on the contrary, the source power exceeds the step propagation velocity, a concave growth facet (001) (Fig. 12b), skeletal growth, and the appearance of twins on the edges of the substrate (Fig. 12c) develop, which is inadmissible. It is very important to achieve matching of the rates of these two processes during homoepitaxy.

6.6 Ehrlich–Schwoebel barrier

The difference in the energy barriers for adatom movement through a step and diffusion along an atomic terrace is called the Ehrlich–Schwoebel (ES) barrier. It determines the possibility of adatom movement between the terraces of two growth layers across the edge of the step (processes 11 and 12 in Fig. 5). Its nature is illustrated by Fig. 16a. Even in metals, the ES barrier greatly affects the growth mechanism, and it is even more significant in crystals with directed, covalent bonds, which include diamond. A distinction is made between a positive ES barrier when an adatom rises from the lower to the upper terrace (process 12 in Fig. 5) and a negative ES barrier for the descent of an adatom (process 11 in Fig. 5). When an adatom moves from the lower to the upper terrace, it first enters a potential well at the edge of the step (Fig. 16a), where, as already noted, it is bound to neighboring atoms by a large number of bonds [240]. Therefore, the positive ES barrier is almost always greater than the negative one, and the diffusion channel up the staircase of steps, at least under the conditions of CVD diamond growth, is completely suppressed.

The physical reason for the ES barrier is illustrated for diamond in Fig. 16b [194]. Since the sp^3 bonds are directional, and the thermal vibrations of the atoms at typical CVD growth temperatures are still small compared to the Debye temperature of diamond (2000 K), both the positive and negative barriers are fairly high, contrary to the opinion presented in [188]. Unfortunately, the ES barriers for diamond have not yet been determined experimentally, although a technique (developed for Pb) is available [241].

At the key, initial stage of epitaxy, the ratio of the polished surface relief to the direction of the growth step staircase is of great importance. Even on a well-polished (without scratches or chips) diamond surface, a system of wavy, smooth, and parallel grooves is found [242], and their cross section is unchanged over a length of many micrometers (Fig. 17a). For the {100} facet polished in the soft direction ⟨100⟩, the groove width is 20–100 nm, and the depth is 4–12 nm, which is significantly greater than the thickness of the atomic layer [243]. The atomic layers on such a surface are schematically shown in Fig. 17b.

As can be seen in Fig. 17b, a continuous staircase of steps required for epitaxy is not formed across the grooves on a wavy surface. Smoothing the wavy surface requires the transfer of adatoms from one atomic step to another, one of the channels of which is shown in Fig. 17b by a curved arrow. However, this mechanism is hindered by the high ES barrier. If the source of layer growth (the edge of the plate) is located

as shown by the blue line in Fig. 17b, nothing prevents the development of a staircase of growth steps along the grooves, and then wavy material grows from the edges of the plate or from other sources of layer growth (Figs 12a and 15a). If, however, the source of layered growth is located as shown by the red line in Fig. 17b, the development of a staircase of steps across the grooves is not possible. That is why in such a case the growth of a continuous homoepitaxial film is delayed (the incubation period is sometimes as long as many hours), until local sources of layered growth are formed (mainly on the upper ribs of the wavy relief) in the form of hillocks (Fig. 12a) yielding various morphological elements in the form of 'scales,' 'toles,' etc. This is one of the factors of poor reproducibility of the results of epitaxy on various substrates.

7. Morphological instability of layered growth

Back in 1997, the main manifestations of morphological instability of homoepitaxial diamond growth by the CVD method were described in [244]: ''A systematic study of the morphology of (001) homoepitaxial diamond films grown by microwave CVD shows that the growth of these films strongly depends on such parameters as the vicinal angle of the substrate, the concentration of methane, and the growth temperature. With an increase in the vicinal angle, the morphology of the growth surface changes from mound growth to the formation of macrosteps. Step growth provides a higher growth rate than mound growth. This shows that step growth plays a key role in diamond growth. It is assumed that mound growth occurs during the nucleation of two-dimensional clusters on terraces at a low step density. At the same time, step growth in the $\langle 110 \rangle$ direction is realized at a high step density. The formation of macrosteps is more clearly expressed at a lower temperature of 875 °C than at 1200 °C. Apparently, single-domain layered step growth provides more perfect films with a lower concentration of defects than other growth modes. It seems that step growth requires an increase in the vicinal angle, a decrease in the methane concentration, and an increase in the substrate temperature.''

Many theoretical studies involving a rich mathematical apparatus and Monte Carlo growth modeling (a good review is presented in [245]) are devoted to the development of the vicinal surface morphology during the layer-by-layer growth of monatomic crystals. They are supported by experimental examples from the epitaxial growth of metals (Pt, Au, Ag, Rh, Cu, etc.), Si, Ge, SiC, oxides, salts, organic crystals, etc. [168, 246–250]. The main manifestations of morphological instability during crystal growth are described in [251]. They include the grouping of steps (with the formation of macrosteps), meandering of steps, growth of hillocks and mounds, and formation of depressions (craters).

Characteristic examples of the listed phenomena for molecular beam epitaxy of GaN and AlN are reported in [252–254]. All these phenomena constitute the main difficulty in growing perfect crystals of large sizes, especially from the gas phase. Diamond, alas, is no exception. Well-developed theoretical analysis and modeling of all manifestations of layered crystal growth [168, 240, 245–250] lends hope for solving the problems of diamond homoepitaxy. For the diamond facet {100}, all manifestations of morphological instability are described in detail in many experimental papers, for example, in [29, 34, 67, 233, 244, 255, 256].

The morphology of the epitaxial film is mainly influenced by the growth conditions, and primarily by supersaturation [257]. It is no coincidence that, in [258], all other things being equal, with a small variation in the methane content in the gas mixture of 6, 6.2, 6.4, and 7%, homoepitaxial films of a completely different morphology grew. This points to the need for precise selection and long-term stability of supersaturation, ensuring homogeneity of the driving force of crystallization over the entire growth surface.

Development of the diamond surface morphology (001), the appearance of areas close to the {111} facets, inevitably leads to the emergence of {111} growth layers and, ultimately, the formation of twin growths (see Section 7.5). This is the failure of epitaxy. For this reason, the goal of CVD diamond homoepitaxy technology should be reoriented from achieving the maximum growth rate regime to finding conditions and regimes for long-term and stable epitaxy by (001) layers.

7.1 Grouping of growth steps

The main manifestations of the behavior of growth steps are their grouping and meandering [259–261].

Grouping of steps is understood as an accumulation of elementary atomic steps, approximately parallel to each other (Fig. 18a). The surface profile showing elementary steps, a grouping of steps B_1, and a grouping of steps with the formation of a macrostep B_2 is shown in Fig. 18b [262]. The ends of B_2 macrosteps, which are clusters of elementary steps, generally do not have an orientation corresponding to facets with simple Miller indices. Over time, they can turn into 'true' macrosteps, the ends of which are crystallographic facets F with simple Miller indices.

The main factor determining the grouping of steps is the diffusion of adatoms along the growth terrace. This phenomenon is especially important for the growth of crystals from the gas phase and in molecular beam epitaxy. Two-dimensional diffusion of adatoms (process 2 in Fig. 5) occurs along the atomic terrace, interrupted by their desorption (process 3 in Fig. 5). Therefore, the concentration of adatoms decreases with increasing distance to the edge of the upper step. The diffusion length of adatoms along an atomic step is usually 2–3 orders of magnitude greater than the interatomic distance. Steps that are separated by a distance much greater than the diffusion length of adatoms do not influence each other. If, however, the distance between the steps is less than the diffusion length of adatoms, the flow of adatoms to such steps decreases compared to faraway steps [263]. Such positive feedback leads to a slowdown in the movement of nearby steps and forms 'traffic jams' of steps (a grouping of steps and macrosteps, as shown in Fig. 18), otherwise figuratively called 'shock waves' [262]. All processes during crystal growth are random in nature; therefore, a small change in the activity of the source of growth steps, protrusions on the edges of steps and similar fluctuations quickly develop due to such positive feedback, resulting in a grouping of steps. If a cluster of steps has already formed, the lower step in it tends to break away from the cluster, but then this layer catches up to the next cluster.

The rise of adatoms (process 11 in Fig. 5) and their descent (process 12 in Fig. 5) over the edge of the terrace along with the detachment of an adatom from the corner of the step (process 9 in Fig. 5) weaken the effect of positive feedback during step grouping. However, at high ES barriers, mechanisms 11 and 12 in Fig. 5 are not operative, and in these cases step grouping (B_1) is often observed (and in such monatomic

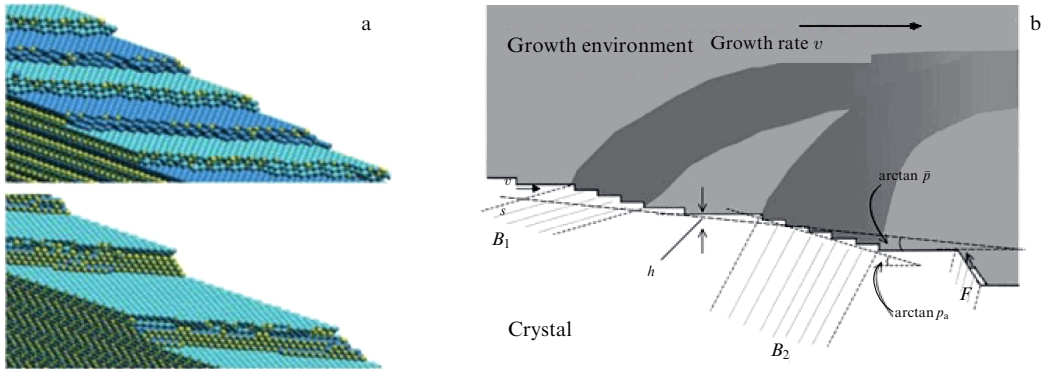

Figure 18. (a) Schematic representation of development of a group of atomic steps on a vicinal facet with appearance of macrosteps. (b) Stepped profile of a vicinal facet with atomic steps, with a cluster of steps B_1, a macrostep B_2, and a macrostep of different crystallographic orientation with nucleating growth layer F.

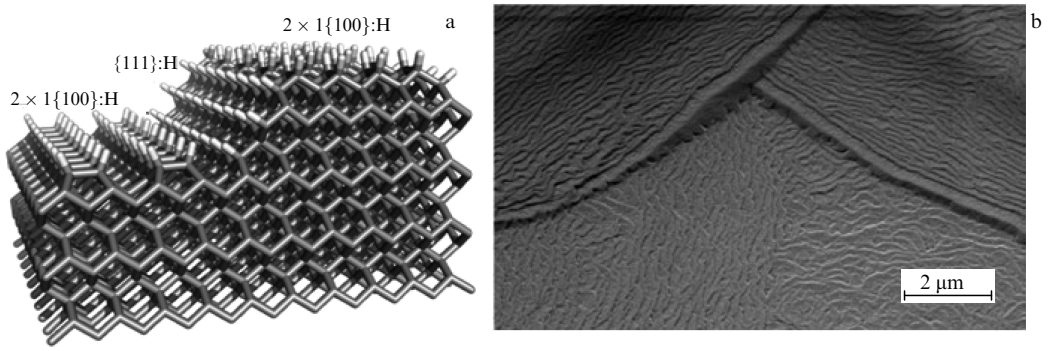

Figure 19. (a) Schematic view of hydrogenated facet of diamond C{100}:H 2×1 with a polyatomic step, the slope of which forms {111} facet. Here, directions of dimer bonds are different on upper and lower terraces: parallel to step on upper one and perpendicular to step on lower one. (b) SEM image of (001) facet of diamond as a result of CVD growth with addition of 4% N_2 to gas mixture.

crystals as metals, Si, Ge, and diamond, almost always), often reaching the formation of macrosteps (B_2) and even macrosteps with the formation of a new facet F (Figs 18b and 19a) [193]. According to the data from [240, 264, 265], the main contribution to the step grouping is made by the positive barrier ES, which is insurmountable in the case of CVD epitaxy of diamond due to the presence of a deep energy well for adatoms at the edge of the step. Depending on the growth mode, the height of the macrosteps can stabilize or constantly increase with time [266, 267].

Active impurities strongly affect the development of the step grouping [268]. One of the proposed mechanisms is that impurities that hinder the development of steps are adsorbed in the corners of atomic terraces: the wider the terrace, the longer it is subject to the adsorption of impurities. The higher the density of impurities, the more of them that accumulate in the corner of the step, the more they reduce the rate of propagation of steps, and the greater the accumulation of steps [262]. Here again, positive feedback is observed. This is illustrated by Fig. 19b, showing the grouping of growth steps (B_1), their meandering, and the formation of macrosteps (types B_2 and F) during CVD diamond growth under conditions of nitrogen addition to the growth medium [269]. Following [65, p. 110], the authors believe that another reason for the mutual inhibition of step motion may be the collision of growth steps coming from different directions from different sources of layered growth, as in Fig. 19b.

The greatest risk in the grouping of steps is the formation of a macrostep with the emergence of a new facet F (Figs 18b and 19a). As Fig. 19a shows, such a facet will most likely be type {111}, and this creates a hazard of twinning. Thus, on two F-type macrosteps, clearly visible in the upper half of the image in Fig. 19b, with a high probability, over time, {111} growth layers are formed, followed by twin growths [270]. The mechanism for the formation and development of such a growth twin on the (001) face is described in [271]. It is precisely these twins that are most often formed during CVD epitaxy of diamond on the (001) face [272], which can be seen below in Fig. 27a.

The way step clusters capture impurities and defects is different than that of single steps. This is exhibited in the banding of the grown crystal, which is detected in luminescence [262]. It also turns out that dislocation clusters are confined to macrosteps [238].

7.2 Meandering of growth steps

Meandering of growth steps is exhibited in the curved shape of the edges of the growth steps (Fig. 20). It is often observed during epitaxy of crystals, especially metals, grown from the vapor phase at low temperatures (Fig. 20a) [273]. Its source is the positive feedback described in Fig. 9b due to the action of a 2D boundary diffusion layer [259].

At high epitaxy temperatures, the diffusion of adatoms along the step edge (process 5 in Fig. 5) neutralizes the effect of this positive feedback. Therefore, during CVD epitaxy of diamond, meandering occurs only in the case of nitrogen addition to the growth medium (Figs 19b and 20b) [274]. In many studies, in particular in [23, 38, 274], it was shown that the addition of nitrogen enhances meandering and step grouping, but, on the other hand, reduces the formation of

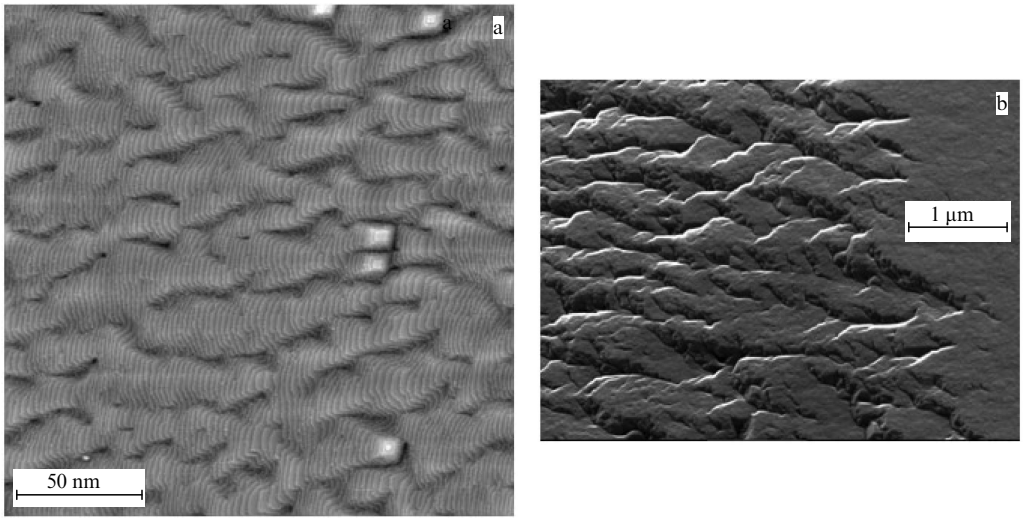

Figure 20. (a) STM topogram of facet vicinal to (001) facet of a Cu single crystal as a result of depositing 18 monolayers at a temperature of 280 K. (b) SEM image of growth layers of (001) facet of diamond as a result of epitaxy with addition of 4% N_2 to gas medium.

hillocks and mounds on the growth surface of CVD diamond. Apparently, the nitrogen adatom or its radical is fixed in the corner of the atomic step (due to the greater number of bonds) and is not capable of diffusion along its edge. In this position, it captures carbon adatoms diffusing along the edge of the step (process 10 in Fig. 5), thus interrupting their diffusion, embedding them into the crystal, simultaneously forming a protrusion on the edge of the step, which ensures meandering.

This hypothesis also provides another clue to understanding the increase in the diamond growth rate in the presence of nitrogen. Under conditions of a low driving force for crystallization, an adatom that has entered the corner of a step (process 4 in Fig. 5) then moves along its corner (process 5 in Fig. 5), but with a high probability it breaks away from the corner (process 9 in Fig. 5), begins to diffuse again along the atomic terrace (process 2 in Fig. 5), and, most likely, desorbs into the gas phase (process 3 in Fig. 5), i.e., will not be built into the crystal. However, the nitrogen atom in the corner of the step captures the carbon adatom moving along the corner, thus preventing its desorption and building it into the crystal. The abundance of protrusions and bends at the edge of such a step also enhances the incorporation of carbon adatoms diffusing along the edge of the step into the crystal (process 6 in Fig. 5). This increases the growth rate of step v and, consequently, the normal growth rate of facet V, according to formula (10).

7.3 Growth craters

These elements of epitaxial diamond morphology in the form of faceted pits, which in dissertation [275] are aptly called growth craters, are not often described in publications. It has been noted that they appear during epitaxy under conditions of low nitrogen concentration, low supersaturation, and high concentration of atomic hydrogen (Fig. 21a) [276]. Under such conditions, the contribution of the diamond etching effect is large, which is why in studies [61, 113, 234, 276] they are called etch pits. However, in appearance and origin, growth craters are fundamentally different from etch pits [113].

Etch pits are obtained by treating diamond in a plasma of pure H_2 [277] or $H_2 + O_2$ [278–280] without hydrocarbon, usually in the same CVD growth reactors. Despite the impression that the manifestations of crystal growth and its etching should be symmetrical, in fact, dislocations, point defects, and impurities manifest themselves in different ways in the two processes. This is due to the different roles of mechanical stresses around them. During growth, they have little effect, but, during etching, their effect is very strong [65, p. 11]. On the {111} facet, the etch pits have a third-order symmetry axis [65, p. 175], while on the {100} facet, a fourth-order symmetry axis (Fig. 21a, b). Plasma etching is widely used to reveal defects in the near-surface region of diamond [62]. Under the influence of plasma, generally speaking, the entire surface is etched [277], but the etching rate is higher near defects. There are two types of etch pits: with a pointed bottom (Fig. 21a) and with a flat bottom (Fig. 21b) [65, p. 112]. It has been established that pointed etch pits appear at the sites of dislocations emerging on the surface [281, 282], and this circumstance is widely used to reveal the dislocation structure of diamond and other crystals. Such a pit is formed due to the field of mechanical stresses around the dislocation [123, 283–286]. Pits with a flat bottom are associated with point defects near the surface [65, pp. 112, 287]. On facets with a strong deviation from the [001] vector, a staircase of macrosteps is revealed as a result of etching [279].

It is stated in [113] that, unlike etch pits, growth craters have an eighth-order symmetry axis. A closer examination shows that they actually have two order symmetry axes rotated relative to each other by 45° (Fig. 21a). It should be noted that the growth craters are not uniformly distributed — they are grouped, forming chains and clusters (Fig. 21a).

Growth craters on CVD diamond also differ from pits of growth origin found on the surfaces of natural [288, 289] and HPHT crystals [290], which grow almost exclusively in {111} layers: here, they are formed by outcrops of {111} growth facets on the surface of other crystal facets, similar to those seen in Fig. 24b.

The formation of growth craters is systematically noted during the epitaxy of many crystals [249]. It has been established that the critical factor in their formation is the ES barrier, in this case negative, which does not allow adatoms to descend from the upper atomic step to the lower

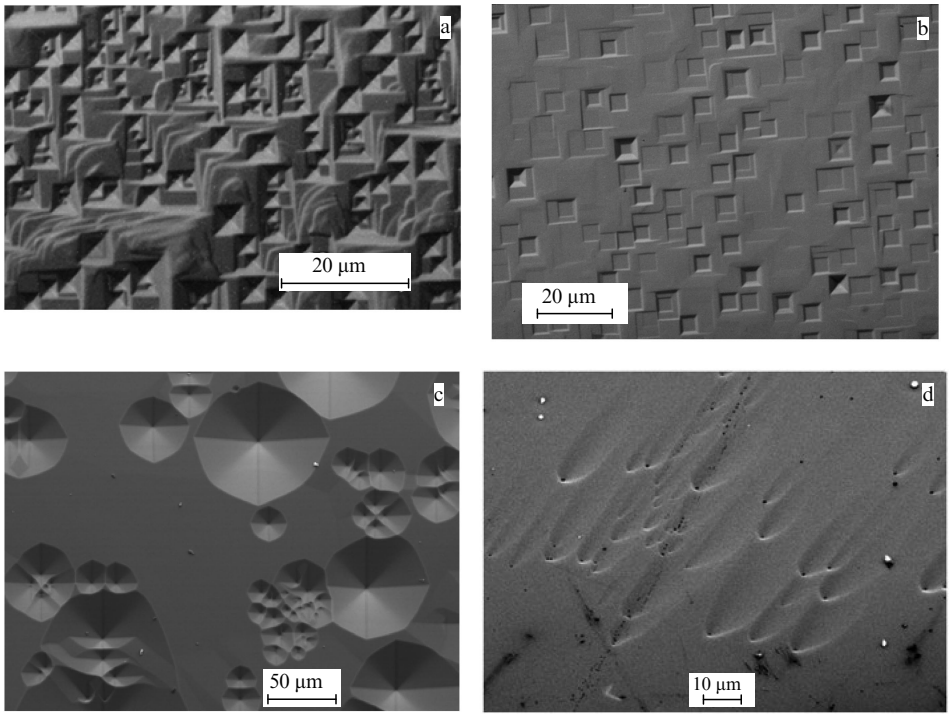

Figure 21. Two types of pits in epitaxial diamond: (a, b) micrographs of etch pits on (001) diamond facet after treatment in hydrogen plasma; (c) SEM image of epitaxial CVD diamond on (001) facet with growth craters; (d) SEM image of probable nuclei of growth craters on (001) facet.

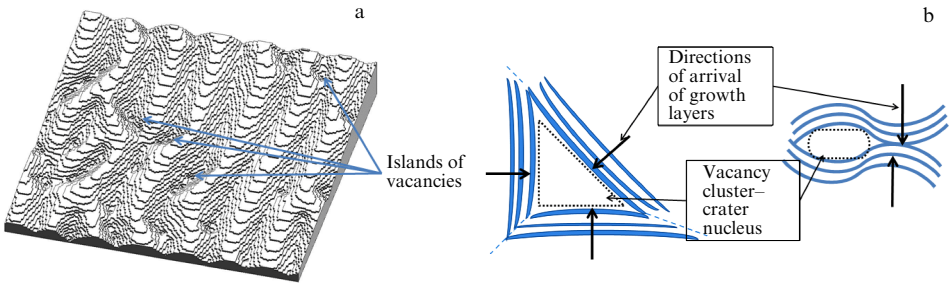

Figure 22. (a) Simulation of layer-by-layer growth of a monatomic metal under meandering conditions and action of an ES barrier. (b) Diagrams of formation of vacancy clusters, nuclei of growth craters, when growth layers converge from different sides.

one. The second factor is the strong meandering of the growth layers. Together, they lead to a situation where the constantly developing tongues of meandering growth layers can close, leaving behind an island of vacancies (as in Fig. 5). This phenomenon is well modeled (Fig. 22a) [291].

The island of vacancies is the nucleation center of a growth crater. As soon as the growth layers coming from several sides form a terrace closed on all sides by higher atomic terraces, adatoms from the overlying terraces can no longer descend into it due to the ES barrier, in this case negative. The initial sizes of such pits can be varied, and their bottom at this stage is flat (Fig. 23). The pit expands due to the growth of new atomic layers around it. As the size of the hole increases, more and more atoms from the gas phase begin to fall into it. They cannot get out of it because of the ES barrier, this time positive. First, they complete the terraces and form stairs of growth layers that form the slopes of the pit. This occurs as a result of the diffusion of adatoms along the terraces and along the corners of the growth steps and explains why the bottom of the formed pit becomes pointed, and its slopes acquire clear crystallographic symmetry (Fig. 21a).

In the case of CVD epitaxy of diamond, meandering is not the main source of vacancy island formation, since meandering occurs only in the presence of a noticeable amount of nitrogen (see Section 7.2 and Fig. 20b), and, in this case, as experience shows, craters are not formed. The authors believe that the main reason for the formation of vacancy islands that give rise to craters is the convergence of growth layers from different directions and from different sources of growth layers, which, when closing, can form vacancy islands. This is schematically shown in Fig. 22b. Probable nucleation centers of growth craters (Fig. 21d) are sometimes found on the (001) growth facet at the initial stage of epitaxy with a low methane concentration.

Another source of growth crater formation may be etch pits. The CVD process in a reactor begins with the ignition of a microwave discharge in a gas, and this is always carried out on pure hydrogen at a low pressure (about 10 Torr). Then, the hydrogen pressure is increased, and only after heating the substrate to a temperature corresponding to the selected epitaxy mode is methane supplied. Moreover, the technological recipe for CVD epitaxy of diamond includes preliminary etching of the diamond substrate for several tens of minutes in

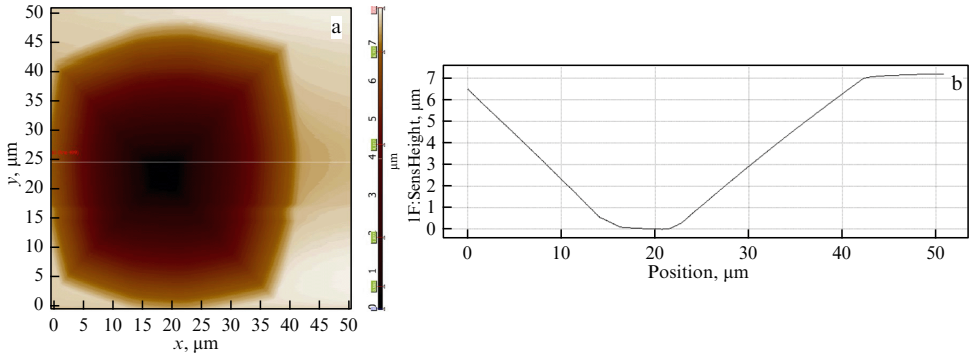

Figure 23. (a) 2D AFM profilogram of epitaxial film region with large growth crater. (b) Surface profile along crater center (shown in panel a as a white line).

pure hydrogen plasma to remove surface contaminants and a thin surface layer of the substrate damaged by polishing. This also contributes to the formation of a staircase of growth steps [292] and, of course, is also accompanied by the formation of etch pits on the substrate surface, as in Fig. 21a, b. It is important not to overdo it. If the etch pits are deep, then, already at this stage, being vacancy islands, they will give rise to growth craters.

The formation of growth craters has been well studied in the epitaxy of many materials, for example, ZnO [293]. This is a crystal of hexagonal syngony; therefore, the pits on its surface (0001) have a symmetry axis of the sixth order. At first, they have a flat bottom, but as the atoms are deposited from the gas phase, the atomic terraces converge towards the center, forming a symmetrical pointed pit with certain slopes of the lateral facets, very similar to the pits shown in Fig. 21a. In study [293], the growth crater is originally called an 'inverted wedding cake.' We will encounter the term 'wedding cake' again when considering burial mounds. A very similar picture is observed in the study of growth craters in CVD epitaxial diamond films on the (001) facet (Fig. 23).

Study [113] measured that the crater walls make an angle of 13.9° with respect to the (001) plane. According to our data, the inclination angle of the lateral sides of the formed growth crater with respect to the (001) plane depends slightly on the direction of the measurement line with respect to the crater symmetry axes and, according to the analysis of AFM scans of several craters, is $18 \pm 1.3°$ (Fig. 23b). The slopes of the formed crater have a symmetrical, epitaxially completed shape (Fig. 21a) — for some reason, the shape of the crater and the inclination angle of the staircase of steps inside it no longer change. It is unclear what determines this angle.

The crater displayed in Fig. 23 has not yet fully formed: its slopes are slightly asymmetrical, and the bottom is still flat. The right part of the profilogram (Fig. 23a) shows that the growth layers came from different sides: from the upper right and from the lower right corners, and this indicates the source of crater formation, consistent with Fig. 22b. The growth layers on the slopes of the pit are also clearly visible.

The appearance of stable pits on the growth surface increases the effect of morphological instability: the growth layers are forced to circumvent the pits, forming tongues, bend, and often close, leaving behind new uncovered clusters of surface vacancies, future new craters. Some of the authors of this review believe that this leads to accelerated, explosive formation of new craters [291]. For this reason, the craters appear almost simultaneously in time and are grouped, forming clusters and chains (Fig. 21a).

The crater expands due to the growth of new layers around it. However, as the size of the crater increases, more and more atoms from the gas phase constantly get into it. They cannot get out of it because of the ES barrier. First, they complete the terraces and form ladders of growth layers that form the slopes of the pit, which clearly indicates the diffusion of adatoms, not only along the atomic terraces, but also along the edges of the growth steps. This explains why the bottom of the formed crater is pointed and its shape is symmetrical, as in Fig. 21a. Subsequently, the adatoms that fall into the pit should form sp^3 material, but there is no room to complete the terraces in the pit. The formed crater begins to get overgrown. This is why some growths appear on the bottom and on the slopes of the craters over time (Fig. 24a). Later {111} growth layers begin to form on the slopes of the crater, and they grow from the bottom up, which suggests increased supersaturation at the bottom of the pits.

The growth of {111} layers on the slopes of the crater has adverse implications. First, as is known, {111} growth layers bring a risk of twinning. In some samples, the pits manage to get overgrown without the formation of twins (Fig. 24b). However, sometimes, especially with increasing supersaturation, twin growths form at the bottom of the growth pits (where the {111} layers grow from), destroying the epitaxy (Fig. 24c, d). Second, even without twinning, the {111} layers that have grown to the edges of the craters are uneven (Fig. 24b). On the (001) facet, they act as new sources of growth layers (001) and, when they overgrow from above, defective areas can be buried in the volume. Third, the convergence of different growth layers during the overgrowth of the pit generates a large number of dislocations [142]. All of these factors are undesirable growth defects that adversely affect the optical and electrophysical properties of the material.

Experience shows that, in the presence of nitrogen (intentionally or unintentionally included in the gas medium), craters do not form [294]. A hypothetical reason is that a nitrogen atom with a large number of free bonds that ends up in the corner of a growth step removes the negative ES barrier [295] in this place and, thus, allows adatoms to descend into the vacancy island (process 11 in Fig. 5), preventing the development of a crater. Craters do not form at relatively high supersaturation either, but then hillocks and mounds are formed.

7.4 Hillocks and mounds

Hillocks and mounds are the most visible and the most undesirable elements of the morphology of CVD single-crystal layers. Therefore, they are described in a large

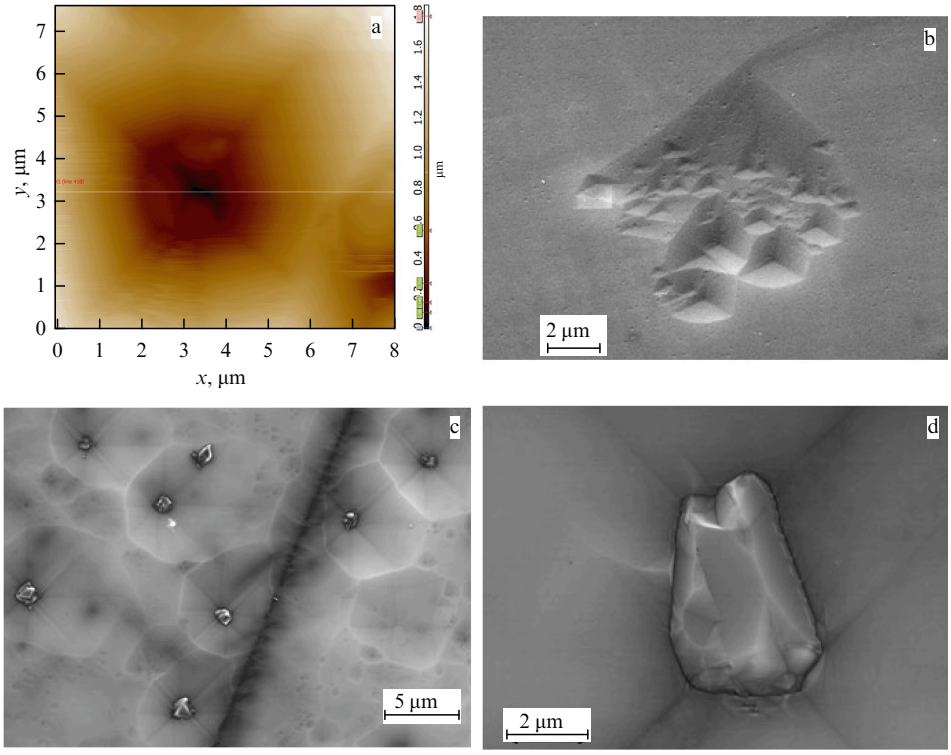

Figure 24. (a) 2D AFM topogram of lower part of growth crater with growths inside it. (b) SEM image of growth crater overgrown with {111} layers. (c, d) SEM images of twin growths at bottom of growth pits.

number of publications on CVD diamond, for example, in [39, 221, 296–298]. They have a square shape. It is necessary to emphasize the morphological difference between a hillock with a pointed top and a mound with a flat top (mound, wedding cake, pyramidal hillocks) (Fig. 25). This difference, however, can not always be understood from a single-stage image [299], because sometimes hillocks with seemingly sharp tops grow over time into mounds with flat tops (Fig. 26).

Mounds are also formed on the diamond facets {111}, but, of course, are triangular in shape [157, 300]. In [201], it was even possible to record on the {111} facet the initial moment of formation of a 2D island, which subsequently can produce a mound with a flat top.

The formation of hillocks and mounds is well known from the epitaxy of a wide variety of materials ranging from monatomic metals (Fig. 25a) to zeolites and organic crystals [301–304]. Very often, truly pointed mounds are formed by screw dislocations, which, in full accordance with the BCF theory [169], provide spiral growth of the crystal under conditions of a small driving force of crystallization. An example is the right mound in Fig. 25a, which clearly shows the development of monatomic growth layers along a spiral. For an adatom on the terrace of such a spiral, there is always an open path for diffusion both upward and downward along the spiral of the atomic layer. It is this mechanism that is responsible for the growth of crystals under conditions of low supersaturation, i.e., perfect crystals grow around screw dislocations.

At the same time, the left mound in Fig. 25a is formed by a stack of isolated atomic layers, the diffusion of adatoms between which is impossible in the case of a high ES barrier. This form of mound is figuratively called a 'wedding cake' by some authors [304, 305]. In epitaxial CVD diamond, there are also hillocks with sharp tops and mounds with flat tops [306]. They differ in the shape of the upper part (as in Fig. 25); however, both of them, but especially mounds, are undesir-

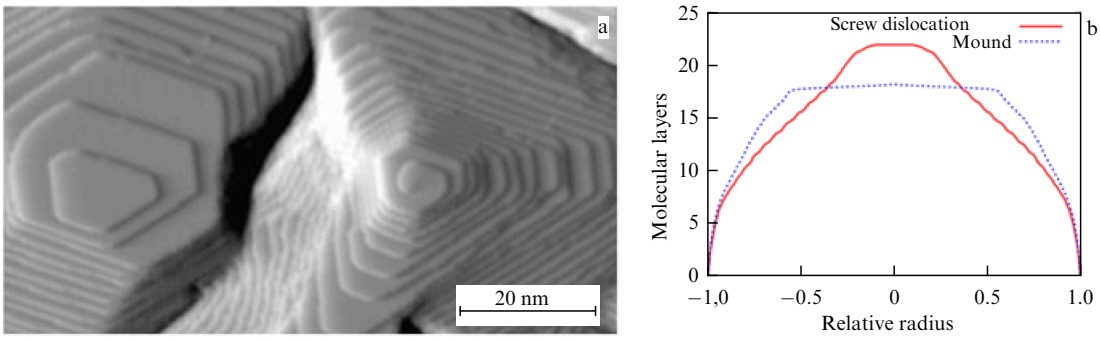

Figure 25. (a) STM topogram of a flat-topped mound and a sharp-topped hillock during epitaxial growth of Pt. (b) Cross section of a sharp-topped hillock and a flat-topped mound.

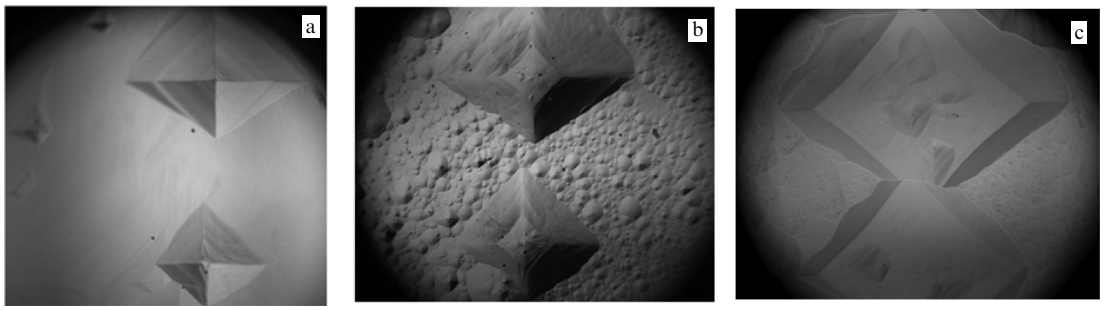

Figure 26. Optical images of development of two mounds on (001) facet in center of substrate shown in Fig. 11a during growth for 15 h (a), 25 h (b), and 50 h (c). Horizontal frame size is 500 μm.

able in the process of diamond epitaxy, since twin growths are inevitably formed on their slopes over time (Fig. 27). On the growth facet {111} of CVD diamond, hillocks are reliably identified around screw dislocations [157]. The growth of perfect diamonds from solutions (natural and HPHT crystals) is mainly driven by screw dislocations on the {111} facets [65, pp. 180–182; 228, pp. 155–158]. There is evidence of growth around a screw dislocation on the {100} facet of HPHT diamond [65, p. 185]. However, although many dislocations emerge on the {100} growth facet of CVD diamond (and they have been well studied [90, 93, 123, 129, 283, 286, 307–311]), the authors have not yet found any reliable evidence of the formation of mounds with a spiral structure (as in Fig. 25a on the right) around them on the (001) facet of CVD diamond, either in publications or in personal observations. True, spiral structures are often observed on the growth facets of {100} crystallites of polycrystalline films. Screw dislocations emerging on the (001) facet of single-crystal CVD diamond have not yet been detected either [282, 312–314]. This may be explained by the crystal structure of dislocations emerging on the (001) facet [307]. Otherwise, the spiral structures around the dislocations are formed by very thin layers that are difficult to distinguish and are possibly even monoatomic, to which the STM technique has not yet been applied.

The layers of the mounds grow due to the arrival of adatoms from the underlying terraces (process 4 in Fig. 5). Sometimes, the mounds grow to the extent that new smaller mounds are formed on their flat tops (Fig. 26b, c).

The mechanism of mound formation has been well studied experimentally in metal epitaxy [315]. First, as a result of random fusion of atoms on an atomically smooth terrace, a single-layer 2D nucleus is formed (as in the upper part of Fig. 5). The nucleation of two-dimensional domains on atomic terraces during CVD growth of diamond was discovered in [177]. If its size happens to exceed the critical one [287], it continues widening due to the addition to its periphery of adatoms diffusing along the adjacent terrace (process 4 in Fig. 5) and its surface area increases. Such a 2D nucleation center is not yet a mound. If it turns out to be close to the advancing growth terrace, it can absorb it, forming a protrusion. However, if atoms from the gas phase fall on a solitary 2D nucleation center and if it has not yet adjoined the advancing nearest growth layer, the adatoms cannot leave its surface due to the ES barrier, in this case negative. They form a second layer (process 13 in Fig. 5); at this moment, a mound is formed. The formed mounds protrude above the growth surface and are fed from the enlarged angular sector of the 3D boundary diffusion layer, i.e., they turn out to be under the effect of an increased driving force of crystallization, which increases the probability of the nucleation of a new 2D nucleation center on its flat top, giving rise to a new atomic layer. All these factors maintain accelerated growth of the mounds.

On the vicinal facets (001), we also see conical mounds, which act as local sources of layer growth and give rise to 'scales' (Fig. 12a). Some of them are probably nevertheless formed around screw dislocations. Figure 27b clearly shows that twin growths are formed primarily near the tops of mounds and hillocks. An explanation is that, according to modeling [305] and numerous measurements (mainly by the STM method), during epitaxy of various crystals near the top of a mound or on the edge of a flat top of a mound, the angle of inclination of the steps of the growth layers is maximal

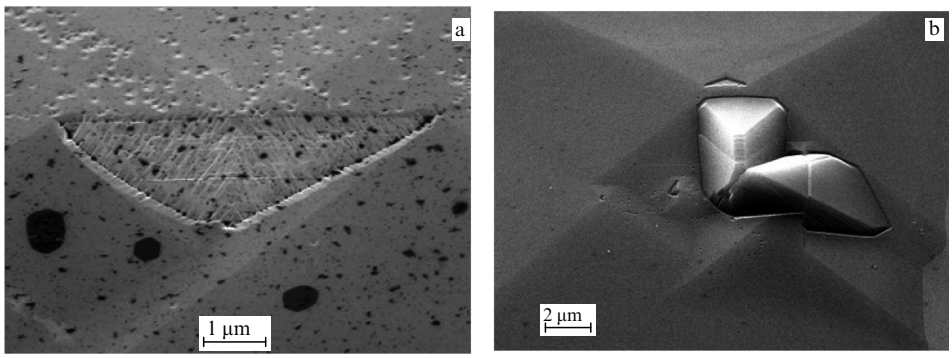

Figure 27. (a) SEM image of formation of {111} growth layers near top of a mound on (001) growth facet of a diamond. Twinning will inevitably begin on {111} layer over time. (b) SEM image of twins on top of the mound.

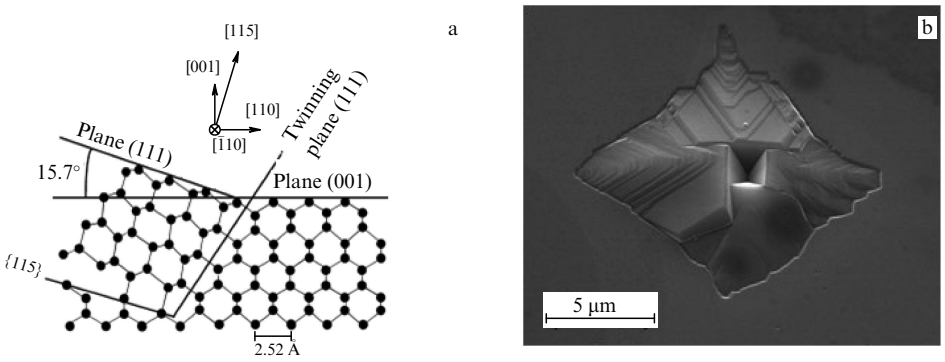

Figure 28. (a) Atomic configuration of a growth twin. (b) SEM image of twin growths near top of mound on facet vicinal to (001) facet of CVD diamond.

(Fig. 25a, b). In such a place, according to the mechanism described in Fig. 18b, a {111} growth layer may spontaneously form. In Fig. 27a, it has a triangular shape. The {111} layer will inevitably begin to twin over time [299, 316], as can be seen in Fig. 27b.

Very spectacular growth patterns were obtained on artificial round mounds (originally designed for a different purpose) made on a (001) diamond substrate using photolithography in [317–319]. The growth of such mounds occurs primarily on the sides due to the addition of adatoms from the lower atomic terraces. On the flat top of the mound, twin growths quickly formed, primarily near the edges, which again indicates a higher driving force for crystallization in the indicated places and a large slope of the growth surfaces. The slopes of the mounds acquired a crystallographic faceting. As in the case of growth craters, this observation again provides reliable evidence of the possibility of adatom displacement along the corners of growth steps (process 5 in Fig. 5). As it turns out, the crystal structure of such mounds is literally riddled with a huge number of dislocations and other defects, although the reason is not clear. The same is indicated by cathodoluminescence topography maps [206], including those made at the free exciton wavelength of 235 nm. In the upper part of the image in Fig. 27a, a large number of small pits can be seen. They are the pointed square etch pits described in Section 7.3. They are always observed at the end of the CVD process, since it is also performed in steps: first, the methane supply is stopped, then the hydrogen pressure is gradually reduced, and only then is the microwave radiation switched off. As a result, the substrate is exposed to almost pure hydrogen plasma for some time. However, as described in Section 7.3, such etch pits are formed at the sites of dislocation protrusions. This observation clearly demonstrates the defective structure of the mound.

The development of the morphology of epitaxial facets has been well studied in the homoepitaxy of metals due to the options of using STM technology with atomic resolution [171, pp. 537, 561]. These studies show that the mounds are formed on wide atomic terraces in full accordance with the above-described model of their formation and development. From this observation, three important conclusions can be drawn for the epitaxy of crystals (including diamond). First, growth on facets with a small vicinal angle to (001), i.e., with wide atomic terraces, increases the probability of mound formation [195]. Second, it is necessary to avoid growth modes that lead to a strong grouping of steps, producing separate wide atomic steps (as in Fig. 18). Third, all other things being equal, an increase in supersaturation increases the probability of mound formation.

In [320], to reduce the probability of mound formation, a multi-stage procedure of chemical and plasma cleaning and high-temperature annealing of the diamond substrate preceding epitaxy was proposed. It is based on the concept that mounds and twins develop due to substrate surface defects (such as in Fig. 14a). However, this approach was tested in [320] only for growing films several micrometers thick with still weak morphology development. While fully supporting the opinion that careful preparation of the substrate for epitaxy (see Section 6.3 and [321]) is required, we nevertheless emphasize that the formation of mounds and hillocks is controlled by alternative mechanisms.

Based on our own experience and analysis of publications, we consider mounds to be the main enemies of stable diamond epitaxy by the CVD method. It has become clear from experience that mounds are formed at an enhanced driving force for crystallization, while growth craters (see Section 7.4) are formed at a low one. Based on this, the following empirical recipe can be recommended: under specific growth conditions, select a compromise supersaturation (determined by the methane concentration in the gas mixture) so that mounds are not formed, but at the same time the number of craters is smaller.

7.5 Twinning

Twinning determines the morphology of diamond polycrystalline films [322, 323] and the polycrystalline rim along the perimeter of a single-crystal substrate (Fig. 12b, c). The mechanism for the formation of twins on the {111} facet of diamond is described in [324]. Study [35] showed that the nucleation of a twin on the {111} facet begins with the formation of a 2D cluster of four carbon atoms on it, which subsequently performs as a nucleation center for the spinel twin $\Sigma 3$ {111}. This explains the experimentally observed increase in the probability of twin formation with increasing supersaturation. When a $\Sigma 3$ {111} twin is formed, the distances between the nearest neighboring atoms and even the next neighbors change insignificantly (Fig. 28a). The angles between the bonds of the nearest neighbors alone change. Therefore, the energy of formation of such a twin is small: its estimated value is 0.14 J m^{-2} [325]. Consequently, the energy of the stacking fault formed by two such parallel twins is approximately twice as large, $\sim$ 0.29 J m^{-2}. These are small values that do not constitute a large barrier to twin formation at temperatures characteristic of the CVD process.

From the point of view of the morphology of twinned crystallites, a distinction is made between contact twins and intergrowth twins [326], although at the atomic level twinning always occurs when the crystal lattice is rotated by 60° or,

equivalently, by 180° around the ⟨111⟩ axis parallel to the direction of interatomic bonds. Contact twins are formed on the {111} facet and remain perpendicular to the direction of twinning ⟨111⟩. Intergrowth twins arise on the {111} and {100} facets (Fig. 28a, b), but in this case the plane of the twin is not perpendicular to the ⟨111⟩ direction.

The formation of twins, especially multiple ones, is accompanied by strong mechanical stresses [325] and the formation of a large number of dislocations in the surrounding material [327]. It is the mechanical stresses from multiple twinnings that are mainly responsible for the cracking of the growing CVD diamond substrate. In [328], it is clearly shown that dislocation bundles in the epitaxial material propagate from a stacking fault limited by two twin planes. The main conclusion is that twinning is ultimately the main obstacle to diamond homoepitaxy.

8. Selecting crystallographic faceting of substrate

As early as the dawn of diamond epitaxy technology by the CVD method [82, 207, 234, 276], it was noted that, on the facet close to (001), during the epitaxy process, such undesirable morphological elements as pits, macrosteps, mounds, and hillocks develop very rapidly, which inevitably lead to the appearance of twin growths (see Figs 27 and 28). It has also been noted that more stable growth is observed on substrates with a large vicinal angle [329]. In many studies on crystal epitaxy, increasing the vicinal angle is proposed to suppress morphological instability [330, 331]. In the case of CVD diamond, various optimal vicinal angles (usually 2–5°) and various directions of deviation of the [001] vector are reported. The direction of deviation of the [001] vector, as has now become clear (see Section 6.3), determines which edges of a conventional plate-shaped substrate will operate as sources of layered growth, and how the growth layers will spread relative to the polishing grooves (see Fig. 17). With a significant deviation of the [001] vector in the ⟨100⟩ direction, the sources of layered growth are two edges (Fig. 12a), and with a significant deviation in the ⟨110⟩ direction, three edges (Fig. 15a). It is quite clear that, with a small vicinal angle on wide atomic terraces, the probability of forming mounds, the main enemies of epitaxy, is high. This allows us to approximately indicate the undesirable range of vicinal angles in Fig. 8 as a blue circle around the {001} direction. It is clear that the real angular size of such a circle depends on the driving force of crystallization, which is determined by supersaturation.

The upper value of the angle of deviation of the growth facet from (001) is determined by the risk of forming {111} growth facets. The {111} facets are inclined relative to the (001) facet by 54.7°. The assumed regions of acceptable vicinal angles are shown in the region in Fig. 8 with blue inner and red outer boundaries. At least from observations of growth craters (see Section 7.3), we know that the permissible deviation angle can be fairly large (∼ 18°).

In this regard, attention is drawn to the {311} facets, which deviate from the (001) plane by 25.2° in the {311} directions (Figs 13a and 29) and in Fig. 8 fall within the assumed region of permissible deviations. Moreover, spontaneous formation of {311} facets is often observed during diamond homoepitaxy (Fig. 1b) [64, 71–75, 211], and morphologically stable growth is observed on polished {311} facets, although often with the formation of macrosteps (Figs 7 and 13b) [74–76]. This fact has not yet been explained, especially since the macroscopic {311} facets are actually formed by {100}-type layers, as can be seen in Fig. 13b and shown schematically in Fig. 29. We only note that the {311} facet has the maximum density of {100} growth steps (see Fig. 29), while the {211} facet has the maximum density of {111} growth steps (see Fig. 29). This implies that faceting the substrate with {211} facets should be avoided.

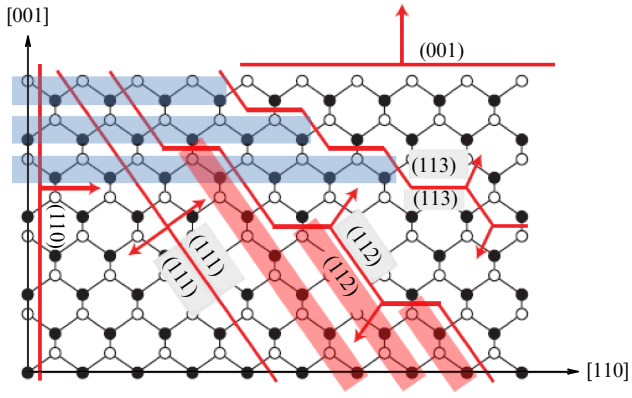

Figure 29. Cross section of diamond crystal lattice by (110) plane. Crystallographic planes (001), (110), (111), (113), and (112) are marked. (001) layers are shown in blue, and (111) layers, in pink.

There is no certainty yet that stable growth can be achieved with only {311} facets on a substrate faceted by a tetragontrioctahedron, as proposed in [72] (see Fig. 13). Experiments in [73] on a cylindrical substrate with an upper facet (113) were in fact not pure due to the development of other facets on the side surface of the substrate. However, in the current situation, the use of {311} facets in cutting the substrate still seems promising.

9. Ways to overcome challenges of CVD technology

The urgent task of CVD diamond homoepitaxy technology is to achieve long-term, morphologically stable growth of crystalline perfect diamond. At present, growth layers from different layer sources at the junction points inevitably produce structurally imperfect material with a dislocation network. Particularly defective local areas originate from morphological imperfections (buried craters, mounds, and twins). Sooner or later, epitaxy is interrupted by the formation of twins on the growth surface and the development of a polycrystalline rim along the perimeter of the substrate.

Correct diagnosing is a necessary but, alas, not sufficient condition for solving the problem. In our opinion, the situation is difficult but not hopeless. A solution should be looked for in the theory of layered growth and the experience of epitaxy of other crystals. In [253, 254], various manifestations of morphological instability of homoepitaxy of trinitrides (GaN, AlN) with morphological elements completely analogous to diamond are described, and ways of suppressing their formation are indicated. The list of the main ones includes increasing the temperature, reducing supersaturation to increase the diffusion length of adatoms along atomic terraces and enhancing the etching of two-dimensional nuclei, and reducing the width of the terraces of growth steps

(increasing the vicinal angle). All these measures, in our opinion, are applicable to diamond epitaxy [332].

We now consider the methods proposed for achieving morphological stability as applied to epitaxy of high crystalline perfection diamond (with a focus on low-nitrogen-type IIa diamond) using the CVD method (primarily with microwave excitation).

9.1 Preparation of substrate

1. Use of nonplanar substrates faceted from all sides instead of plates with unpolished side facets. The faceting should ensure the most uniform distribution of the driving force of crystallization over all growth facets, taking into account the large spatial inhomogeneity of the key growth parameters of the plasma.

2. Removal of all growth facets from crystallographic facets {111} and {100}. The use of {311} facets looks promising.

3. Creation by faceting of a minimum number of controlled sources (preferably linear) of growth layers to minimize the convergence of layers from different growth sources.

4. Provision of growth steps on all polished facets during cutting {100} to obtain layered growth.

5. High-quality polishing of all substrate facets, without scratches and chips. The polishing grooves should be directed along the staircase of growth steps. Removal of the surface layer damaged by polishing (IRE, CMP, annealing) without increasing the roughness.

6. Protection of nongrowth substrate facets from the growth of a polycrystalline rim. This can be achieved by placement in a substrate holder with a recess or masking with a neutral coating or faceting that minimizes the supply of growth radicals to the side facets (with inclination angles greater than 90°).

9.2 Selection of growth conditions

Technologists' efforts are focused on the selection of optimal epitaxy parameters. Additionally, it is proposed to:

1. Go beyond the usual ranges of growth parameters, in particular, growth at an elevated substrate temperature [211]. For example, reported in [333] is the use of not only high pressures of the gas mixture (up to 350 Torr) but also elevated substrate temperatures (up to 1500 °C) to increase the probability of decay of dimers and 2D nucleation centers, and to increase the diffusion length of adatoms on atomic terraces. It may also be possible to at least partially overcome the ES barrier. The temperature range above 1650 K (1377 °C) seems especially promising. As indicated in Section 5, the maximum concentration of methyl radicals is reached at a temperature in the gas phase. The use of growth temperatures above 1377 °C should change the negative gradient (towards the substrate) of the methyl radical concentration in the boundary diffusion layer described in Section 5 to positive. However, in accordance with Fig. 3b, the concentration gradient of atomic hydrogen remains negative. As a result, a local increase in the gas temperature near any protrusion on the growth surface should reduce supersaturation and hence the local driving force of crystallization and the growth rate. This should create negative feedback that inhibits the development of irregularities.

2. Increase the concentration of atomic hydrogen near the growth surfaces, in particular, by increasing the discharge power.

3. Achieve the most uniform possible concentration of methyl radicals and atomic hydrogen near the growth surfaces of the substrate.

4. Match the powers of the layer growth sources and the lateral growth rate of the layers by precisely selecting supersaturation.

5. Optimize etching in hydrogen (possibly with a small addition of oxygen) before the start of growth, sufficiently short for deep etch pits not to form and sufficiently long to form a staircase of growth steps.

6. Reduce the substrate temperature gradient along the height to reduce mechanical stresses in the crystal volume.

7. Add neutral elements to the gas mixture, preferably not incorporated into diamond, to influence reactions during layer-by-layer growth. This issue is virtually skipped in this review, but it seems that, in addition to nitrogen, boron, oxygen, silicon, and argon, many other additives can be tested. It should be taken into account that many chemical elements (like oxygen) can significantly affect both the growth plasma and the mechanism of layer-by-layer diamond growth, while they are hardly incorporated into the diamond crystal lattice. Even if they are incorporated to a minor extent, they have little effect on its electrical and optical properties.

10. Conclusions

High-quality CVD epitaxy of diamond (as well as other crystals) is driven exclusively by the layer-by-layer mechanism. In diamond epitaxy, {111} and {100} atomic layers are observed. On the {111} facets, only very slow epitaxy is possible. As the growth rate increases, twinning occurs on such facets. The experience of growing various crystals and the tools developed to describe the layered mechanism of their growth allowed us to analyze the mechanisms of morphological instability of the layered growth of CVD diamond on a facet close to (001). Its manifestations include the grouping of steps, their meandering, and the formation of growth craters and mounds. All of them lead to the development of the growth surface relief and an increase in the angle of inclination of its individual sections relative to [001], which provokes the formation of {111} layers, fraught with twinning. Especially hazardous in this regard are mounds, near the tops of which twins are sooner or later formed. The main sources of morphological instability of CVD epitaxy of diamond are a large gradient of key growth parameters in the boundary diffusion layer and the ES barrier.

The sources of layered growth and the ladder of growth steps play a fundamental role in the layered growth of diamond. When cutting the substrate, it is necessary to provide a minimum number of controlled sources of layered growth, preferably in the form of ribs, and a staircase of growth steps. The urgent need to develop a technology for preparing growth surfaces of a diamond substrate that meets the requirements of high-quality homoepitaxy has long been overdue.

It is now apparent that stable epitaxy is impossible on facets close to {111} and {100}, and on substrates in the form of (001) plates. The paradox is that the growth should occur in (001) layers but with a large angular deviation from the (001) facet. Growth on {311} facets looks promising. In addition, the substrates should have an optimal facet and position relative to the plasma cloud, minimizing the role of the gradient of the growth parameters of the boundary layer and its heterogeneity. Taking this into account, diamond

homoepitaxy through the CVD method should be focused on finding an optimal growth mode that does not necessarily provide the maximum growth rate, but rather the maximum — ideally multi-day-long — duration of stable growth.

References

1. DeVries R C, Badzian A, Roy R *MRS Bull.* **21** (2) 65 (1996)
2. Spitsyn B V, Deryagin B V "Sposob narashchivaniya granei almaza" ("Method to grow diamond facets"), USSR Inventor's Certificate No. 339134 dated 10.07.1956; *Byull. Izobret.* (17) 323 (1980)
3. Eversole W G, Kenmore N Y, US Patent 3030187, patented Apr. 17, 1962; https://patents.google.com/patent/US3030187A/en; US Patent 3030188, patented Apr. 17, 1962; https://patents.google.com/patent/US3030188A/en
4. Derjaguin B V et al. *J. Cryst. Growth* **2** 380 (1968)
5. Spitsyn B V, Bouilov L L, Derjaguin B V *J. Cryst. Growth* **52** 219 (1981)
6. Matsumoto S et al. *Jpn. J. Appl. Phys.* **21** L183 (1982)
7. Angus J C *Diamond Relat. Mater.* **49** 77 (2014)
8. Kasu M *Prog. Cryst. Growth Charact. Mater.* **62** 317 (2016)
9. Goodwin D G *J. Appl. Phys.* **74** 6888 (1993)
10. Derkaoui N et al. *J. Phys. D* **47** 205201 (2014)
11. Gicquel A et al., in *Comprehensive Hard Materials* Vol. 3 (Ed.-in-Chief V K Sarin) (Oxford: Elsevier, 2014) p. 217, https://doi.org/10.1016/B978-0-08-096527-7.00047-7
12. Scott C D et al. *J. Thermophys. Heat Transfer* **10** 426 (1996)
13. Harris S J, Goodwin D G *J. Phys. Chem.* **97** 23 (1993)
14. Krasnoperov L N et al. *J. Phys. Chem.* **97** 11787 (1993)
15. Butler J E, Woodin R L *Philos. Trans. R. Soc. London A* **342** 209 (1993)
16. Brinza O et al. *Phys. Status Solidi A* **204** 2847 (2007)
17. Gracio J J, Fan Q H, Madaleno J C *J. Phys. D* **43** 374017 (2010)
18. Wörner E, Wild C, in *Comprehensive Hard Materials* Vol. 3 (Ed.-in-Chief V K Sarin) (Oxford: Elsevier, 2014) p. 365, https://doi.org/10.1016/B978-0-08-096527-7.00052-0
19. Haubner R *ChemTexts* **7** 10 (2021)
20. Bradley C E et al. *npj Quantum Inform.* **8** 122 (2022)
21. Aharonovich I et al. *Adv. Mater.* **24** OP54 (2012)
22. Balmer R S et al. *J. Phys. Condens. Matter* **21** 364221 (2009)
23. Chayahara A et al. *Synthesiology Engl. Ed.* **3** 259 (2010)
24. Khmelnitskiy R A *Phys. Usp.* **58** 134 (2015); *Usp. Fiz. Nauk* **185** 143 (2015)
25. Tallaire A et al. *Phys. Status Solidi A* **202** 2059 (2005)
26. Tallaire A et al. *Diamond Relat. Mater.* **14** 249 (2005)
27. Mallik A K *J. Coat. Sci. Tech.* **3** 75 (2016)
28. Schwander M, Partes K *Diamond Relat. Mater.* **20** 1287 (2011)
29. Liu J et al. *Diamond Relat. Mater.* **46** 42 (2014)
30. Sutcu L F et al. *J. Appl. Phys.* **71** 5930 (1992)
31. Nad S, Charris A, Asmussen J *Appl. Phys. Lett.* **109** 162103 (2016)
32. Eaton-Magaña S, Shigley J E *Gems Gemol.* **52** 222 (2016)
33. Polushin N I et al. *Processes* **8** 666 (2020)
34. Achard J et al. *Phys. Status Solidi A* **9** 1651 (2012)
35. Butler J E, Oleynik I *Philos. Trans. R. Soc. London A* **366** 295 (2008)
36. Delclos S et al. *Diamond Relat. Mater.* **9** 346 (2000)
37. Gu Y et al. *Diamond Relat. Mater.* **24** 210 (2012)
38. Chayahara A et al. *Diamond Relat. Mater.* **13** 1954 (2004)
39. Zhao Y et al. *Cryst. Res. Technol.* **53** 1800055 (2018)
40. Wu G, Chen M-H, Liao J *Diamond Relat. Mater.* **65** 144 (2016)
41. Nad S, Asmussen J *Diamond Relat. Mater.* **66** 36 (2016)
42. Charris A, Nad S, Asmussen J *Diamond Relat. Mater.* **76** 58 (2017)
43. Feng M et al. *J. Cryst. Growth* **603** 127011 (2023)
44. Nad S, Gu Y, Asmussen J *Diamond Relat. Mater.* **60** 26 (2015)
45. Yang B et al. *J. Mater. Sci.* **55** 17072 (2020)
46. Nagase M et al. *Jpn. J. Appl. Phys.* **51** 070202 (2012)
47. Li F et al. *Crystals* **7** 114 (2017)
48. Li Y et al. *Diamond Relat. Mater.* **101** 107574 (2020)
49. Silva F et al. *Diamond Relat. Mater.* **18** 683 (2009)
50. McCauley T S, Vohra Y K *Appl. Phys. Lett.* **66** 1486 (1995)
51. Chen J et al. *J. Cryst. Growth* **484** 1 (2018)
52. Gicquel A et al. *J. Phys. III France* **6** 1167 (1996)
53. Gicquel A et al. *Chem. Phys.* **398** 239 (2012)
54. Derkaoui N et al. *J. Appl. Phys.* **115** 233301 (2014)
55. Grotjohn T et al. *Diamond Relat. Mater.* **14** 288 (2005)
56. Shu G et al. *J. Cryst. Growth* **486** 104 (2018)
57. Hassouni K, Silva F, Gicquel A *J. Phys. D* **43** 153001 (2010)
58. Angus J C et al. *Philos. Trans. R. Soc. London A* **342** 195 (1993)
59. Lombardi G et al. *Plasma Sources Sci. Technol.* **14** 440 (2005)
60. Lombardi G et al. *J. Appl. Phys.* **98** 053303 (2005)
61. Muchnikov A B et al. *Diamond Relat. Mater.* **19** 432 (2010)
62. Ma Z et al. *Diamond Relat. Mater.* **66** 135 (2016)
63. Gordon M H et al. *J. Appl. Phys.* **89** 1544 (2001)
64. Tallaire A et al. *C.R. Physique* **14** 169 (2013)
65. Sunagawa I *Crystals. Growth, Morphology, and Perfection* (Cambridge: Cambridge Univ. Press, 2005) https://doi.org/10.1017/CBO9780511610349
66. Anthony T R *Vacuum* **41** 1356 (1990)
67. Wang X et al. *Materials* **12** 3953 (2019)
68. Battaile C C et al. *J. Chem. Phys.* **111** 4291 (1999)
69. Hei L F et al. *Diamond Relat. Mater.* **30** 77 (2012)
70. Miyoshi K "Chemical-Vapor-Deposited Diamond Film", NASA/TM—1999-107249 (Hanover, MD: NASA Center for AeroSpace Information, 1999)
71. Brinza O et al. *Phys. Status Solidi A* **205** 2114 (2008)
72. Silva F et al. *J. Cryst. Growth* **310** 187 (2008)
73. Silva F et al. *Diamond Relat. Mater.* **17** 1067 (2008)
74. Janssen G et al. *J. Cryst. Growth* **125** 42 (1992)
75. Snail K A et al. *J. Cryst. Growth* **137** 676 (1994)
76. Li S et al. *Carbon* **145** 273 (2019)
77. Khmelnitsky R A, Talipov N Kh, Chucheva G V *Sinteticheskii Almaz dlya Elektroniki i Optiki* (Synthetic Diamond for Electronics and Optics) (Moscow: IKAR, 2017)
78. Achard J et al. *Diamond Relat. Mater.* **16** 685 (2007)
79. Asmussen J *Appl. Phys. Lett.* **93** 031502 (2008)
80. Lyu J et al. *Surf. Eng.* **35** 91 (2019)
81. van Enckevort W J P et al. *Surf. Coat. Technol.* **47** 39 (1991)
82. Takeuchi D et al. *Diamond Relat. Mater.* **9** 231 (2000)
83. Okushi H *Diamond Relat. Mater.* **10** 281 (2001)
84. Ri S-G et al. *J. Cryst. Growth* **235** 300 (2002)
85. Bauer T et al. *Diamond Relat. Mater.* **14** 266 (2005)
86. Bauer T et al. *Phys. Status Solidi A* **203** 3056 (2006)
87. Miyatake H et al. *Diamond Relat. Mater.* **16** 679 (2007)
88. Naamoun M et al. *Phys. Status Solidi A* **210** 1985 (2013)
89. Li H, in *Thin Films and Epitaxy* (Handbook of Crystal Growth, Second ed., Vol. IIIA Basic Techniques, Eds T F Kuech) (Amsterdam: Elsevier, 2015) p. 605, https://doi.org/10.1016/B978-0-444-63304-0.00014-7
90. Davies N et al. *J. Phys. Conf. Ser.* **281** 012026 (2011)
91. Ohmagari S et al. *Diamond Relat. Mater.* **48** 19 (2014)
92. Maida O et al. *Diamond Relat. Mater.* **17** 435 (2008)
93. Tallaire A et al. *Diamond Relat. Mater.* **33** 71 (2013)
94. Li Y et al. *Vacuum* **206** 111529 (2022)
95. Schreck M et al. *J. Appl. Phys.* **127** 125102 (2020)
96. Chatei H et al. *Diamond Relat. Mater.* **6** 505 (1997)
97. Hassouni K et al. *Plasma Sources Sci. Technol.* **10** 61 (2001)
98. Brinza O et al. *Phys. Status Solidi A* **204** 2847 (2007)
99. Muchnikov A B et al. *Diamond Relat. Mater.* **20** 1225 (2011)
100. Vikharev A M et al. *J. Phys. D* **45** 395202 (2012)
101. Mokuno Y et al. *Diamond Relat. Mater.* **19** 128 (2010)
102. Yamada H et al., in *Materials Challenges and Testing for Manufacturing, Mobility, Biomedical Applications and Climate* (Eds W Udomkichdecha et al.) (Cham: Springer Intern. Publ., 2014) p. 97
103. Aida H et al. *Diamond Relat. Mater.* **75** 34 (2017)
104. Girshick S L et al. *Plasma Chem. Plasma Process.* **13** 169 (1993)
105. Tallaire A et al. *Phys. Status Solidi A* **208** 2028 (2011)
106. Hemawan K W, Hemley R J *J. Vac. Sci. Technol. A* **33** 061302 (2015)
107. Bolshakov A P et al. *Diamond Relat. Mater.* **62** 49 (2016)
108. Yamada H, Chayahara A, Mokuno Y *Diamond Relat. Mater.* **87** 143 (2018)
109. Muehle M et al. *Diamond Relat. Mater.* **79** 150 (2017)
110. Bolshakov A P et al. *Mater. Today Commun.* **25** 101635 (2020)
111. Williams O A, Jackman R B *Diamond Relat. Mater.* **13** 557 (2004)
112. Issaoui R et al. *Phys. Status Solidi A* **208** 2023 (2011)
113. Liu J et al. *Vacuum* **155** 391 (2018)
114. Issaoui R et al. *Diamond Relat. Mater.* **94** 88 (2019)
115. Yokota Y et al. *Diamond Relat. Mater.* **12** 295 (2003)

116. Zhang Q et al. *Diamond Relat. Mater.* **20** 496 (2011)
117. Belousov M E et al. *Chem. Vapor Deposition* **18** 302 (2012)
118. Han X et al. *Materials* **13** 4510 (2020)
119. Yamada H et al. *Diamond Relat. Mater.* **15** 1383 (2006)
120. Liu J et al. *Diamond Relat. Mater.* **46** 42 (2014)
121. Janssen G et al. *Diamond Relat. Mater.* **1** 789 (1992)
122. Sergeichev K F, Lukina N A, Arutyunyan N R *Plasma Phys. Rep.* **45** 551 (2019); *Fiz. Plazmy* **45** 513 (2019)
123. Martineau P et al. *Phys. Status Solidi C* **6** 1953 (2009)
124. Martineau P M et al. *J. Phys. Condens. Matter* **21** 364205 (2009)
125. Feng Z B et al. *Diamond Relat. Mater.* **19** 1453 (2010)
126. Umezava H et al. *Diamond Relat. Mater.* **20** 523 (2011)
127. Willems B, Tallaire A, Achard J *Diamond Relat. Mater.* **41** 25 (2014)
128. Mayr M et al. *Phys. Status Solidi A* **211** 2257 (2014)
129. Boussadi A et al. *Diamond Relat. Mater.* **83** 162 (2018)
130. Stehl C et al. *Appl. Phys. Lett.* **103** 151905 (2013)
131. Yan C et al. *Proc. Natl. Acad. Sci. USA* **99** 12523 (2002)
132. Tallaire A et al. *Diamond Relat. Mater.* **15** 1700 (2006)
133. Su Y et al. *J. Cryst. Growth* **351** 51 (2012)
134. Liang Q et al. *Cryst. Growth Des.* **14** 3234 (2014)
135. Yamada H, Chayahara A, Mokuno Y *Diamond Relat. Mater.* **101** 107652 (2020)
136. Liang Q et al. *Diamond Relat. Mater.* **18** 698 (2009)
137. Meng Y et al. *Proc. Natl. Acad. Sci. USA* **105** 17620 (2008)
138. Liang Q et al. *J. Superhard Mater.* **35** 195 (2013)
139. Mokuno Y et al. *Diamond Relat. Mater.* **14** 1743 (2005)
140. Muehle M et al. *Diamond Relat. Mater.* **42** 8 (2014)
141. Eaton-Magaña S et al. *Minerals* **11** 177 (2021)
142. Tallaire A et al. *Diamond Relat. Mater.* **33** 71 (2013)
143. Tallaire A et al. *Diamond Relat. Mater.* **20** 875 (2011)
144. Isberg J et al. *Science* **297** 1670 (2002)
145. Friel I et al. *Diamond Relat. Mater.* **18** 808 (2009)
146. Martineau P M et al. *J. Phys. Condens. Matter* **21** 364205 (2009)
147. Teraji T *Phys. Status Solidi A* **203** 3324 (2006)
148. Goodwin D G, Butler J E, in *Handbook of Industrial Diamonds and Diamond Films* (Eds M A Prelas, G Popovici, L K Biglow) (Boca Raton, FL: CRC Press, 1997) p. 527, https://doi.org/10.1201/9780203752807
149. Dischler B, Wild C (Eds) *Low-Pressure Synthetic Diamond. Manufacturing and Applications* (Berlin: Springer, 1998)
150. Nazare M H, Neves A J (Eds) *Properties, Growth and Applications of Diamond* (Emis Datareviews Ser., 26) (London: INSPEC, 2001)
151. Asmussen J, Reinhard D K (Eds) *Diamond Films Handbook* (New York: M. Dekker, 2002) https://doi.org/10.1201/9780203910603
152. Nebel C E, Ristein J (Eds) *Thin-Film Diamond I* (Semiconductors and Semimetals, Vol. 76) (New York: Academic Press, 2003)
153. Teraji T, in *Physics and Applications of CVD Diamond* (Eds S Koizumi, C Nebel, M Nesladek) (Weinheim: Wiley-VCH, 2008) p. 29, https://doi.org/10.1002/9783527623174.ch3
154. Butler J E, Cheesman A, Ashfold M N R "Recent progress in the understanding of CVD growth of diamond", in *CVD Diamond for Electronic Devices and Sensors* (Eds R S Sussmann) (Chichester: J. Wiley, 2009)
155. Butler J E et al. *J. Phys. Condens. Matter* **21** 364201 (2009)
156. Friel I, in *Optical Engineering of Diamond* (Eds R P Mildren, J R Rabeau) (Weinheim: Wiley-VCH Verlag, 2013) p. 35, https://doi.org/10.1002/9783527648603.ch2
157. Tokuda N, in *Novel Aspects of Diamond. From Growth to Applications* (Topics in Applied Physics, Vol. 121, Eds N Yang) (Heidelberg, 2015) p. 1, https://doi.org/10.1007/978-3-030-12469-4_1
158. Koizumi S, Umezawa H, Pernot J, Suzuki M (Eds) *Power Electronics Device Applications of Diamond Semiconductors* (Duxford: Woodhead Publ., 2018)
159. May P W *Philos. Trans. R. Soc. London A* **358** 473 (2000)
160. Arnault J-C, Saada S, Ralchenko V *Phys. Status Solidi Rapid Res. Lett.* **16** 2100354 (2022) https://doi.org/10.1002/pssr.202100354
161. Hayashi K et al. *Diamond Relat. Mater.* **5** 1002 (1996)
162. Hayashi K et al. *Appl. Phys. Lett.* **68** 1220 (1996)
163. Tyagi P K et al. *Diamond Relat. Mater.* **15** 304 (2006)
164. Harris S J, Belton D N *Thin Solid Films* **212** 193 (1992)
165. Okushi H *Diamond Relat. Mater.* **10** 281 (2001)
166. Lukins P B, Zareie M H, Khachan J *Appl. Phys. Lett.* **78** 1520 (2001)
167. Godbole V P et al. *Appl. Phys. Lett.* **71** 2626 (1997)
168. Jeong H-C, Williams E D *Surf. Sci. Rep.* **34** 171 (1999)
169. Uwaha M *Prog. Cryst. Growth Charact. Mater.* **62** 58 (2016)
170. Frenklach M, Skokov S *J. Phys. Chem. B* **101** 3025 (1997)
171. Ibach H *Physics of Surfaces and Interfaces* (Berlin: Springer-Verlag, 2006) https://doi.org/10.1007/3-540-34710-0
172. Mankelevich Yu A, May P W *Diamond Relat. Mater.* **17** 1021 (2008)
173. Eckert M, Neyts E, Bogaerts A *Cryst. Growth Des.* **10** 4123 (2010)
174. Butler J E et al. *J. Phys. Condens. Matter* **21** 364201 (2009)
175. Harris S J *Appl. Phys. Lett.* **56** 2298 (1990)
176. Harris S J, Belton D N *Thin Solid Films* **212** 193 (1992)
177. Tsuno T et al. *Appl. Phys. Lett.* **64** 572 (1994)
178. Kuang Y et al. *Appl. Phys. Lett.* **67** 3721 (1995)
179. Bobrov K et al. *Phys. Rev. B* **68** 195416 (2003)
180. Foord J S, Loh K P, Jackman R B *Surf. Sci.* **399** 1 (1998)
181. Harris S J, Goodwin D G *J. Phys. Chem.* **97** 23 (1993)
182. Tamura H et al. *Phys. Rev. B* **62** 16995 (2000)
183. Krasnoperov L N et al. *J. Phys. Chem.* **97** 11787 (1993)
184. Battaile C C, Srolovitz D J, Butler J E *J. Cryst. Growth* **194** 353 (1998)
185. Skokov S, Weiner B, Frenklach M *J. Phys. Chem.* **98** 7073 (1994)
186. Netto A, Frenklach M *Diamond Relat. Mater.* **14** 1630 (2005)
187. Cheesman A, Harvey J N, Ashfold M N R *J. Phys. Chem. A* **112** 11436 (2008)
188. May P W et al. *J. Appl. Phys.* **108** 114909 (2010)
189. Liu X et al. *Appl. Surf. Sci.* **362** 387 (2016)
190. Williams M D G "Modelling {100} CVD diamond growth using kinetic Monte Carlo", Doctoral Thesis (Bristol: Univ. of Bristol, 2022)
191. Frenklach M, Skokov S *J. Phys. Chem. B* **101** 3025 (1997)
192. Larsson K, Carlsson J-O *Phys. Rev. B* **59** 8315 (1999)
193. Richley J C, Harvey J N, Ashfold M N R *J. Phys. Chem. C* **116** 7810 (2012)
194. May P W et al. *J. Phys. Condens. Matter* **21** 364203 (2009)
195. van Enckevort W J P et al. *Surf. Coat. Technol.* **47** 39 (1991)
196. Wild Ch, Herres N, Koidl P *J. Appl. Phys.* **68** 973 (1990)
197. van Enckevort W J P et al. *Diamond Relat. Mater.* **4** 250 (1995)
198. Clausing R E et al. *Diamond Relat. Mater.* **1** 411 (1992)
199. D'Evelyn M P, Graham J D, Martin L R *Diamond Relat. Mater.* **10** 1627 (2001)
200. Tallaire A et al. *Diamond Relat. Mater.* **41** 34 (2014)
201. Nishitani-Gamo M et al. *J. Mater. Res.* **14** 3518 (1999)
202. Tallaire A et al. *Diamond Relat. Mater.* **41** 34 (2014)
203. Tsuno T et al. *J. Appl. Phys.* **75** 1526 (1994)
204. Tokuda N et al. *Jpn. J. Appl. Phys.* **53** 04EH04 (2014)
205. Lazea A et al. *Phys. Status Solidi A* **209** 1978 (2012)
206. Teraji T, Mitani S, Ito T *Phys. Status Solid. A* **198** 395 (2003)
207. Tsuno T et al. *Jpn. J. Appl. Phys.* **35** 4724 (1996)
208. Watanabe H et al. *Diamond Relat. Mater.* **8** 1272 (1999)
209. Stekolnikov A A, Furthmüller J, Bechstedt F *Phys. Rev. B* **68** 205306 (2003)
210. Lesik M et al. *Diamond Relat. Mater.* **56** 47 (2015)
211. Janssen G et al. *J. Cryst. Growth* **125** 42 (1992)
212. Bales G S, Zangwill A *Phys. Rev. B* **41** 5500 (1990)
213. Green D S et al. *Science* **259** 1726 (1993)
214. Silva F et al. *J. Phys. Condens. Matter* **21** 364202 (2009)
215. Cappelli M A et al. *Plasma Chem. Plasma Process.* **20** 1 (2000)
216. Ma J et al. *J. Appl. Phys.* **104** 103305 (2008)
217. May P W, Mankelevich Yu A *MRS Online Proc. Library* **1282** 302 (2010)
218. Gicquel A et al. *Chem. Phys.* **398** 239 (2012)
219. Clausing R E et al. *Diamond Relat. Mater.* **1** 411 (1992)
220. Menon P M et al. *Diamond Relat. Mater.* **7** 1201 (1998)
221. Vikharev A L et al. *Mater. Today Commun.* **22** 100816 (2020)
222. May P W, Mankelevich Yu A *J. Phys. Chem. C* **112** 12432 (2008)
223. De Sio A et al. *Diamond Relat. Mater.* **34** 36 (2013)
224. Wild C et al. *Diamond Relat. Mater.* **2** 158 (1993)
225. Teraji T et al. *Phys. Status Solidi A* **212** 2365 (2015)
226. Burton N C et al. *Proc. R. Soc. Lond. A* **449** 555 (1995)
227. Nad S, Gu Y, Asmussen J *Rev. Sci. Instrum.* **86** 074701 (2015)
228. Bokii G B et al. *Prirodnye i Sinteticheskie Almazy* (Natural and Synthetic Diamonds) (Exec. Ed. I I Shafranovskii) (Moscow: Nauka, 1986)
229. Nad S, Asmussen J *Diamond Relat. Mater.* **66** 36 (2016)
230. Friel I et al. *Diamond Relat. Mater.* **18** 808 (2009)
231. Kato Y et al. *Appl. Phys. Express* **6** 025506 (2013)

232. Muchnikov A B et al. *Phys. Status Solidi A* **212** 2572 (2015)
233. Widmann C J et al. *Diamond Relat. Mater.* **64** 1 (2016)
234. Achard J et al. *J. Phys. D* **40** 6175 (2007)
235. Luo H et al. *Int. J. Extrem. Manuf.* **3** 022003 (2021)
236. Tarutani M et al. *Appl. Phys. Lett.* **68** 2070 (1996)
237. Du Y et al. *Nanomaterials* **12** 741 (2022)
238. Mayr M et al. *Phys. Status Solidi A* **212** 2480 (2015)
239. Geng C-W et al. *Acta Phys. Sinica* **67** 248101 (2018)
240. Bellmann K et al. *J. Cryst. Growth* **478** 187 (2017)
241. Li S-C et al. *Phys. Rev. B* **74** 195428 (2006)
242. Couto M et al. *Appl. Surf. Sci.* **62** 263 (1992)
243. Moseler M, Pastewka L, Hird J, in *Comprehensive Hard Materials* Vol. 3 (Ed.-in-Chief V K Sarin) (Oxford: Elsevier, 2014) p. 81, https://doi.org/10.1016/B978-0-08-096527-7.00042-8
244. Lee N, Badzian A *Diamond Relat. Mater.* **6** 130 (1997)
245. Misbah C, Pierre-Louis O, Saito Y *Rev. Mod. Phys.* **82** 981 (2010)
246. Politi P et al. *Phys. Rep.* **324** 271 (2000)
247. Krug J *Physica A* **313** 47 (2002)
248. Kallunki J, Krug J *Europhys. Lett.* **66** 749 (2004)
249. Michely T, Krug J *Islands, Mounds, and Atoms*: *Patterns and Processes in Crystal Growth Far from Equilibrium* (Berlin: Springer, 2004)
250. Krug J, in *Multiscale Modeling in Epitaxial Growth* (Intern. Ser. of Numerical Mathematics, Vol. 149, Ed. A Voigt) (Basel: Birkhäuser, 2005) p. 69, https://doi.org/10.1007/3-7643-7343-1_6
251. Gillet F, Pierre-Louis O, Misbah C *Eur. Phys. J. B* **18** 519 (2000)
252. Corrion A L, Wu F, Speck J S *J. Appl. Phys.* **112** 054903 (2012)
253. Kaufmann N A K et al. *J. Cryst. Growth* **433** 36 (2016)
254. Bryan I et al. *J. Cryst. Growth* **438** 81 (2016)
255. Rouzbahani R et al. *Carbon* **172** 463 (2021)
256. Demlow S N, Rechenberg R, Grotjohn T *Diamond Relat. Mater.* **49** 19 (2014)
257. Shu G et al. *CrystEngComm.* **22** 2138 (2020)
258. Zhang P et al. *Coatings* **11** 888 (2021)
259. Pimpinelli A et al. *Phys. Rev. Lett.* **88** 206103 (2002)
260. Krug J, in *Collective Dynamics of Nonlinear and Disordered Systems* (Eds G Radons, W Just, P Häussler) (Berlin: Springer, 2005) p. 5, https://doi.org/10.1007/3-540-26869-3_2
261. Yu Y-M et al. *Appl. Phys. Lett.* **99** 263106 (2011)
262. Chernov A A *J. Cryst. Growth* **264** 499 (2004)
263. Rost M, Šmilauer P, Krug J *Surf. Sci.* **369** 393 (1996)
264. Xie M H, Leung S Y, Tong S Y *Surf. Sci.* **515** L459 (2002)
265. Slanina F, Krug J, Kotrla M *Phys. Rev. E* **71** 041605 (2005)
266. Sato M, Uwaha M *Surf. Sci.* **442** 318 (1999)
267. Tonchev V *Bulgarian Chem. Commun.* **44** 9 (2012)
268. Vollmer J et al. *New J. Phys.* **10** 053017 (2008)
269. Ashkinazi E E et al. *Crystals* **7** 166 (2017)
270. Akutsu N *Phys. Rev. E* **86** 061604 (2012)
271. Tamor M A, Everson M P *J. Mater. Res.* **9** 1839 (1994)
272. Takami T et al. *Surf. Sci.* **440** 103 (1999)
273. Maroutian T, Douillard L, Ernst H-J *Phys. Rev. B* **64** 165401 (2001)
274. de Theije F K, Schermer J J, van Enckevort W J P *Diamond Relat. Mater.* **9** 1439 (2000)
275. Bogdan G "Growth and properties of nearly atomically-flat single crystal diamond prepared by plasma-enhanced chemical vapor deposition and its surface interactions", Doctoral Thesis (Leuven: Katholieke Univ. Leuven, 2007)
276. Achard J et al. *J. Cryst. Growth* **284** 396 (2005)
277. Ivanov O A et al. *Mater. Lett.* **151** 115 (2015)
278. Tallaire A et al. *Phys. Status Solidi A* **201** 2419 (2004)
279. Naamoun M et al. *Phys. Status Solidi A* **209** 1715 (2012)
280. Tsubouchi N, Mokuno Y, Shikata S *Diamond Relat. Mater.* **63** 43 (2016)
281. Tsubouchi N, Mokuno Y *J. Cryst. Growth* **455** 71 (2016)
282. Ichikawa K et al. *Thin Solid Films* **600** 142 (2016)
283. Kato Y et al. *Diamond Relat. Mater.* **23** 109 (2012)
284. Hoa L T M et al. *Cryst. Growth Des.* **14** 5761 (2014)
285. Ichikawa K et al. *J. Appl. Phys.* **128** 155302 (2020)
286. Tallaire A et al. *Cryst. Growth Des.* **16** 2741 (2016)
287. Rodgers W J et al. *J. Chem. Phys.* **142** 214707 (2015)
288. Sunagawa I *J. Cryst. Growth* **99** 1156 (1990)
289. Mironov V P *AIP Conf. Proc.* **2069** 040006 (2019)
290. Palyanov Y N et al. *Cryst. Growth Des.* **9** 2922 (2009)
291. Kallunki J, Krug J *Europhys. Lett.* **66** 749 (2004)
292. Yurov V et al. *Phys. Status Solidi A* **214** 1700177 (2017)
293. Yin X, Geng D, Wang X *Angew. Chem. Int. Ed.* **55** 2217 (2016)
294. Yamada H, Chayahara A, Mokuno Y *Jpn. J. Appl. Phys.* **55** 01AC07 (2016)
295. Leal F F, Oliveira T J, Ferreira S C *J. Stat. Mech.* P09018 (2011)
296. Shao G et al. *Materials* **14** 5964 (2021)
297. Zhao Y et al. *Materials* **12** 2492 (2019)
298. Ramamurti R et al. *Diamond Relat. Mater.* **17** 1320 (2008)
299. Tallaire A et al. *Diamond Relat. Mater.* **17** 60 (2008)
300. Nakano Y et al. *Diamond Relat. Mater.* **125** 108997 (2022)
301. Krug J, in *Nanoscale Phenomena and Structures. Proc. of the Conf. on Nanoscale Phenomena and Structures in Bulk and Surface Phases, Sofia, 2008* (Ed. D Kashchiev) (Sofia: Prof. Marin Drinov Publ. House of BAS, 2008); arXiv:0709.2049
302. Cubillas P, Anderson M W, in *Zeolites and Catalysis*: *Synthesis, Reactions and Applications* (Eds J Čejka, A Corma, S Zones) (Weinheim: Wiley-VCH, 2010) p. 1, https://doi.org/10.1002/9783527630295.ch1
303. Redinger A et al. *Phys. Rev. Lett.* **100** 035506 (2008)
304. Krug J "Pattern formation by step edge barriers: The growth of spirals and wedding cakes", *2007 MRS Fall Meeting and Exhibit, November 26–30, 2007, Boston*
305. Krug J *J. Stat. Phys.* **87** 505 (1997)
306. Tsubouchi N, Ogura M, Makino T *Diamond Relat. Mater.* **97** 107422 (2019)
307. Gaukroger M P et al. *Diamond Relat. Mater.* **17** 262 (2008)
308. Kato Y et al. *Jpn. J. Appl. Phys.* **51** 090103 (2012)
309. Tsubouchi N, Shikata S *Jpn. J. Appl. Phys.* **53** 068010 (2014)
310. Naamoun M et al. *Diamond Relat. Mater.* **58** 62 (2015)
311. Tallaire A et al. *Adv. Mater.* **29** 1604823 (2017)
312. Fujita N et al. *Phys. Status Solidi A* **203** 3070 (2006)
313. Kato Y et al. *Diamond Relat. Mater.* **29** 37 (2012)
314. Sato Y, Miyajima K, Shikata S *Diamond Relat. Mater.* **126** 109129 (2022)
315. Giesen M, Icking-Konert G S *Surf. Sci.* **412–413** 645 (1998)
316. Tsuno T, Imai T, Fujimori N *Jpn. J. Appl. Phys.* **33** 4039 (1994)
317. Lloret F et al. *Phys. Status Solidi A* **213** 12570 (2016)
318. Lloret F et al. *Appl. Phys. Lett.* **108** 181901 (2016)
319. Lloret F et al. *Nanomaterials* **8** 814 (2018)
320. Wang C, Irie M, Ito T *Diamond Relat. Mater.* **9** 1650 (2000)
321. Achard J et al. *Phys. Status Solidi A* **211** 2264 (2014)
322. Buhler J, Prior Y *J. Cryst. Growth* **209** 779 (2000)
323. Delclos S et al. *Diamond Relat. Mater.* **9** 346 (2000)
324. Angus J C et al. *J. Mater. Res.* **7** 3001 (1992)
325. Dorignac D, Delclos S, Phillipp F *Philos. Mag. B* **81** 1879 (2001)
326. Takami T et al. *J. Vac. Sci. Technol. B* **18** 1198 (2000)
327. Sawada H et al. *Diamond Relat. Mater.* **10** 2030 (2001)
328. Tsubouchi N *Appl. Phys. Lett.* **117** 222103 (2020)
329. Ohmagari S et al. *J. Cryst. Growth* **479** 52 (2017)
330. Zauner A R A et al. *J. Cryst. Growth* **210** 435 (2000)
331. Zhou K et al. *J. Cryst. Growth* **371** 7 (2013)
332. Okushi H et al. *J. Cryst. Growth* **237–239** 1269 (2002)
333. Liang Q et al. *Appl. Phys. Lett.* **94** 024103 (2009)